A long non-coding RNA regulates triazole antifungal susceptibility and virulence in *Aspergillus fumigatus*

Nava Raj Poudyal[1,2], Ryan T. Mehlem[2,3], Priyanka Doneparthi[1*], Tabitha Cady[1^], Sven D. Willger[4#], Maximiliano Ortiz[5], Rooksana E. Noorai[5], Jason E. Stajich[6] and Sourabh Dhingra[1,2,7]

[1]Department of Biological Sciences, Clemson University, Clemson, SC 29634, USA
[2]Eukaryotic Pathogen Innovation Center, Clemson University, Clemson, SC 29634, USA
[3]Department of Genetics and Biochemistry, Clemson University, Clemson, SC 29634, USA
[4]Department of Immunology and Infectious Disease, Montana State University, Bozeman, MT 59717, USA
[5]Clemson University Genomics & Bioinformatics Facility, Clemson University, Clemson, SC 29634, USA
[6]Department of Microbiology and Plant Pathology, University of California-Riverside, Riverside, CA 92521, USA

* Present address: Department of Oncology, Georgetown University, Washington, DC, USA, pd771@georgetown.edu

^ Present address: Biology Department, Morrissey College of Arts and Sciences, Boston College, Chestnut Hill, MA 02467, USA, tabithacady@gmail.com

Present address: Independent Researcher, Düsseldorf, Germany, sven.willger@gmail.com

[7]Address correspondence to: sdhingr@clemson.edu

Abstract:

Azole-resistant *Aspergillus* infections are a source of increasing concern with limited alternative therapeutic options. However, as most infections are still caused by azole-susceptible *Aspergillus* strains, there is a need to better understand fungal responses to azole antifungals. To this end, we discover that a long non-coding RNA, *afu-182,* is a major regulator of *cyp51*-independent azole recalcitrant colony growth (ARC). We observe that loss of *afu-182* leads to azole recalcitrant biofilms and poor treated disease outcomes in murine invasive pulmonary aspergillosis models. In contrast, overexpression of *afu-182* significantly reduces fungal burden in animals treated with azole drugs. Whole transcriptome analyses revealed that azole drug treatment leads to an increase in transcripts of genes encoding 7-transmembrane domain proteins of the RTA1 family, and these proteins are negatively regulated by *afu-182*. Two RTA1 family genes downstream of *afu-182* regulation have individual and combined effect in regulating fungal ARC. Taken together, our data show a trans-acting role of the long non-coding RNA *afu-182* in regulating *Aspergillus fumigatus* response to azole drugs both *in vitro* and *in vivo*. These data provide further support for investigating antifungal drug responses beyond minimum inhibitory concentration testing.

47 **Introduction:**

48

49 *Aspergillus fumigatus* causes a spectrum of infections termed as Aspergillosis,
50 mainly in patients with compromised immune systems (1). The patient population most
51 susceptible to infections is those who have acute neutropenia due to underlying conditions
52 or immunotherapies, or patients on long-term steroid use (2, 3). Recent studies have
53 shown that *A. fumigatus* is a significant cause of secondary infections, leading to increased
54 morbidity and mortality in patients with viral infections, including COVID-19 and influenza A
55 virus (4, 5). Importantly, *A. fumigatus* is increasingly a source of infection in tertiary care
56 centers in patients with mild to no immune suppression, highlighting the prevalence of the
57 infection and increase in the patient population that is susceptible to aspergillosis (6). The
58 World Health Organization (WHO) classified *A. fumigatus* as a critical pathogen in 2023 (7).
59 Azoles, polyenes, and echinocandins are the current classes of antifungal drugs
60 available for aspergillosis treatment; azoles are the most widely used (8). Clinically,
61 voriconazole is the frontline therapy; however, posaconazole, itraconazole and
62 isavuconazole are also used (8). Concerningly, azole drug resistance is on the rise (9).
63 Azoles inhibit the sterol 14-α-demethylase gene, *cyp51* (*erg11* in yeast), which leads to
64 accumulation of toxic sterols (10). Molecularly, resistance to azoles is primarily attributed
65 to mutational hotspots in the *cyp51* gene sequence that affect drug-enzyme binding (11);
66 with or without the replication of a 34 base pair or 46 base pair tandem repeat (TR) in the
67 promoter region of the *cyp51a* gene (commonly referred to as TR_{34} and TR_{46}, respectively)
68 (12–14). TRs in promoter regions increase the binding site of transcription factor SrbA,
69 which positively regulates *cyp51a* transcription (15). SrbA also regulates ergosterol
70 biosynthesis by transcriptional regulation of *erg3*, *erg25* and *erg24* genes (16, 17). In
71 addition, transcription factors *rttA* and *atrR* cooperate with SrbA for azole resistance (18,
72 19).
73 SrbA is a class of ER resident sterol regulator binding element protein (SREBP) that,
74 in association with SREBP cleavage activating protein (Scap) and Insulin induced gene
75 (INSIG), regulates cholesterol levels in mammalian cells (20, 21). In *A. fumigatus*, SrbA

76 plays a significant role in the hypoxia response, low iron response, virulence, and azole
77 susceptibility (20); however, a Scap homolog has not been identified in any Eurotiomycete
78 fungus to date, and the Insig homolog *insA* does not regulate SREBPs or subsequent
79 hypoxia response in these fungi (22). In the mammalian system, INSIG senses the
80 accumulation of sterol pathway intermediates and negatively regulates HMG-CoA
81 reductase, thus blocking the rate-limiting step in sterol biosynthesis (23). In *A. fumigatus,*
82 mutations in HMG-CoA reductase (HMG-CoA) have been recently identified in clinical
83 isolates (24–27), and these mutations, especially in the sterol-sensing domain (SSD), are
84 predicted to inhibit sterol intermediate sensing by changing HMG-CoA-Insig stochiometric
85 balance (28). Thus, *insA* provides a feedback mechanism that contributes to azole
86 resistance (28). Interestingly, overexpression (OE) of *insA* reverses the azole resistance in
87 OE HMG-CoA mutants but not in SSD mutants, highlighting the importance of sterol
88 sensing by HMG-CoA (28).
89 In a laboratory setting, drug resistance is defined as a change in minimum inhibitory
90 concentration (MIC) above the clinical cut-off value measured in standardized MIC testing
91 assays (29). Multiple methods are used to determine the MICs of the antifungal drugs in the
92 laboratory setting, including broth microdilution, disk diffusion assay and E-Test strips (29,
93 30), and strains are then classified as susceptible, resistant, tolerant, persistent or
94 exhibiting hetero-resistance (30) based on the ability of all cells or a sub-population of cells
95 to grow at or above MIC (30, 31). Interestingly, we observed that Δ*insA* strains have
96 increased growth in the presence of azoles on solid medium without a change in measured
97 MIC.
98 Here, we show that *afu-182* is an intergenic long non-coding RNA adjacent to *insA*
99 that negatively regulates fungal response to the azole drugs, which is different from
100 previously defined drug responses (30), and is termed here as azole recalcitrant colony
101 growth (ARC). In an animal model of IPA, the Δ*afu-182* strain causes azole recalcitrant
102 infections, whereas OE-182 strains show increased clearance from the lungs when treated
103 with the azole drug, posaconazole.

104 Collectively, we observed that *afu-182* regulates fungal ARC independent of *cyp51*
105 regulation and plays a significant role in azole treatment outcomes, especially in strains
106 classified as azole-susceptible. Thus, our study has uncovered a novel role of fungal ARC in
107 azole susceptibility both *in vitro* and *in vivo*.
108
109 **Results:**
110
111 ***afu-182* contributes to *the insA-mediated* fungal response:**
112
113 The *Aspergillus fumigatus* INSIG homolog, *insA,* was recently shown to play a role in azole
114 drug susceptibility (28). Intriguingly, when grown on solid medium containing sub-MIC
115 voriconazole (0.3µg/ml), itraconazole (0.075µg/ml), or posaconazole (0.03µg/ml) levels of
116 contemporary azole antifungals, the Δ*insA* mutant had increased growth compared to the
117 WT strain (Figure 1). We complemented the Δ*insA* strain with the *insA* gene and 265nt 3'
118 UTR after the translational stop codon. Surprisingly, the complement strain did not revert to
119 the WT ($p>0.05$, shown in bold, Figure 1) but showed similar *insA* mRNA levels (Figure S1). A
120 careful examination of *insA* annotation revealed the presence of long non-coding RNA, *afu-*
121 *182,* as a possible intergenic or anti-sense lncRNA (32–34). Thus, we sought to define the
122 boundary of *insA* mRNA. We did 3' rapid amplification of cDNA ends (3'RACE) analysis(35)
123 and confirmed that *insA* mRNA ends 191 bp after the translational stop codon (Figure S2).
124 To test the functional complementation and the role of *afu-182*, we complemented the
125 Δ*insA* strain with a DNA fragment with *afu-182* (*insA* gene including 676bp after the
126 translational stop codon, resulting in both cis-acting and trans-acting *afu-182*).
127 Interestingly, the complement fragment with cis-acting *afu-182* reduced ARC and partially
128 reverted the strain to WT levels for voriconazole, posaconazole and itraconazole ($p<0.05$ for
129 Δ*insA* and comp-*insA* with cis-acting *afu-182*, One-Way ANOVA, Figure 1). Importantly, no
130 change in MIC was observed for voriconazole as detected by broth microdilution assay or
131 E-test strip (Figure S1). We defined this growth as azole recalcitrant colony growth (ARC),
132 i.e., an increase in fungal colony growth at 0.5x MIC level without a change in MIC. To

133 confirm the mRNA level of *insA* in the complement strains, we used quantitative reverse
134 transcriptase PCR and did not see a difference in the mRNA levels in both
135 complementation strains compared to WT (Figure S1). Additionally, to confirm that the
136 phenotype was not due to the overexpression of *afu-182*, we confirmed the RNA levels of
137 *afu-182* in all strains and did not see significant differences (Figure S1). Taken together,
138 these data suggest that the fungal ARC is a distinct response, and lncRNA *afu-182* plays an
139 important role in azole-mediated ARC in the Δ*insA* strain.
140
141 ***afu-182* is sufficient to regulate fungal ARC**
142
143 As *afu-182* is necessary to revert the *insA-mediated* ARC phenotype, we sought to define
144 the role of *afu-182* in fungal ARC. We made a Δ*afu-182* strain and complemented the null
145 mutant back at its original genomic locus. We also overexpressed *afu-182* RNA using the
146 *gpdA* promoter by fusing the *afu-182* sequence at the transcription start site (TSS) of the
147 glyceraldehyde-3-phosphate dehydrogenase, gpd(A), promoter (36), followed by the *trpC*
148 terminator sequence (T) from *A. nidulans*. We used qPCR to confirm the levels of *afu-182* in
149 the complement and OE strain and the absence of RNA in the Δ*afu-182* strain. Our qPCR
150 data show the absence of *afu-182* transcript in the Δ*afu-182* strain and WT level of
151 expression in the comp-182 strain (p=0.8014, One-Way ANOVA, Figure S3A). We observed a
152 4-fold overexpression in the OE-182 strain (p = 0.0002, One-Way ANOVA, Figure S3A). To
153 assess the role of *afu-182* in fungal ARC, we serially inoculated the strains (10^5-10^2 conidial
154 density) in the absence and presence of 0.25μg/ml voriconazole (0.5x MIC). The *afu-182*
155 null mutant strain showed increased fungal ARC (26% growth ratio increase, One-Way
156 ANOVA, p=0.0078), confirming that *afu-182* lncRNA is necessary to regulate fungal ARC in
157 response to voriconazole (Figures 2A and 2B). No change in the MIC was observed (Figure
158 S3B). The complement strain reverted fungal growth back to WT levels (p=0.7112, One-Way
159 ANOVA), while OE-182 showed decreased fungal ARC (24% decrease in growth ratio,
160 p=0.0131, One-Way ANOVA), suggesting a causal link between *afu-182 levels* and fungal
161 ARC (Figure 2B).

162 It is possible that *afu-182* inhibits fungal germination and not the azole stress
163 response. Thus, we assessed the germination rates in the absence and presence of
164 voriconazole by measuring OD_{600} using a plate reader at 37°C. No significant differences
165 were observed in the germination rates between the strains in either the absence or the
166 presence of Voriconazole (Figures S3C and S3D, respectively). Next, we assessed the role
167 of *afu-182* in fungal ARC post-germination in a biofilm assay. We allowed all strains to
168 germinate and adhere to the abiotic surface (i.e., cell culture plates) for 12 hours. We then
169 washed the fungal biofilms with PBS and then grew the biofilms in the presence of
170 voriconazole (0.2μg/ml) for 8 hours. The final biofilms were washed, stained with crystal
171 violet and de-stained with ethanol as described previously (37). The binding of crystal violet
172 was measured as an indirect measure of fungal biomass. Importantly, the Δ*afu-182* strain
173 formed azole recalcitrant biofilms (41% increase compared to WT, p=0.0049), indicating
174 fungal ARC in biofilms, whereas the OE-182 mutant showed severe and significant
175 impairment in biofilm development after drug treatment (51% decrease compared to WT,
176 p=0.0011) (Figure 2C). No difference across strains was observed in initial biofilm
177 formation after 12 hours (data not shown). Additionally, to understand the role of growth
178 condition-specific role of *afu-182*, we grew AF as liquid submerged cultures in the presence
179 and absence of voriconazole for 48 hours and weighed dry fungal biomass. The Δ*afu-182*
180 strain showed significantly increased biomass (116% increase compared to WT, p=0.0017,
181 One-Way ANOVA), whereas the OE-182 strain showed significant impairment (76%
182 decrease compared to WT, p=0.0211, One-Way ANOVA) (Figure 2D). Thus, our data show
183 that *afu-182* influences fungal ARC in both planktonic and surface-attached cultures (38).
184
185 ***afu-182* regulates pan-azole fungal ARC**
186
187 Voriconazole is the primary choice of drug to treat IPA; however, other azoles are
188 increasingly utilized (8). Given the long side chain of posaconazole, it binds differently to
189 the target enzyme Cyp51 compared to voriconazole (39). Environmental sampling has
190 recovered strains that are voriconazole-resistant but posaconazole and itraconazole-

susceptible due to the increased binding of their long sidechains to stabilize Cyp51 interactions (40). Thus, we aimed to determine if the fungal ARC response is only with voriconazole or if this is a pan-azole response. To test this, we serially inoculated strains (10^5 – 10^2 conidial density) in the presence or absence of posaconazole (0.03μg/ml), itraconazole (0.075μg/ml), and isavuconazole (0.25μg/ml). Our data show increased fungal growth in the Δ*afu-182* mutant for all azoles tested; whereas OE-182 showed decreased growth for all azoles ($p<0.05$, One-Way ANOVA, Figures 3A-3G), without a change in MIC (Figures 3H and S1), suggesting *afu-182* regulates pan-azole ARC. To assess the recalcitrance, we inoculated our strains in the presence of 0.4μg/ml voriconazole, which inhibited WT growth, while the Δ*afu-182* strain showed robust growth, indicating that fungal ARC adaptation allows AF to grow at levels approaching MIC (Figure 3I); however, all strains failed to grow at 2x MIC (data not shown).

Loss of *afu-182* results in an azole recalcitrant infection in a murine model of invasive pulmonary aspergillosis.

To test the role of *afu-182* during infection, we used a corticosteroid model of invasive pulmonary aspergillosis (41). We challenged mice with 2 x 10^6 spores of the respective strains and monitored mice for 14 days for survival (Figure 4A, schematic). We did not see a difference in survival rates across strains, indicating that *afu-182* does not play a role in virulence in this murine model (Figure 4B, log-rank test, p-value 0.1166). We did not see a qualitative difference in fungal growth or histopathology as determined by GMS and H&E staining, respectively (Figure 4C). We next assessed the impact of *afu-182* loss on azole treatment outcome. Posaconazole was selected due to its higher bioavailability in the absence of grapefruit juice compared to voriconazole in mice (42, 43). Mice were challenged as previously described (41) for a survival assay and were treated with sub-therapeutic levels of posaconazole (5mg/kg) at 24, 48 and 72 hours of infection. Mice were observed for 14 days for survival (Figure 4D, schematic). Mice challenged with Δ*afu-182* strains had significantly more adverse outcomes compared to WT ($p = 0.0103$, log-rank

220 test) (Figure 4E). Thus, the Δ*afu-182* strain that is as virulent as WT in the absence of drug,
221 is recalcitrant to treatment in the presence of the azole drugs. Importantly, treatment of all
222 strains with 20mg/kg posaconazole resulted in non-detectable levels of fungal burden for
223 all strains, indicating that the strain is not drug resistant *in vivo* (data not shown).
224 Additionally, we challenged and treated mice and harvested lungs after 72 hours (Figure 4F,
225 schematic). We measured the fungal DNA as previously described (42). Our data indicate a
226 significantly higher fungal burden in mice challenged with the Δ*afu-182* strain (p=0.0159,
227 Mann-Whitney U-test) and a significantly reduced fungal burden in mice challenged with
228 OE-182 strain (p=0.0159, Mann-Whitney U-test) upon azole treatment (Figure 4G); however,
229 survival of animals infected with OE-182 strain and treated with posaconazole was not
230 different compared to WT (p=0.4065, log-rank test, Figure 4E).
231
232 **RNA levels of *afu-182* are negatively regulated by azole drugs, and Inherent *afu-182***
233 **levels determine fungal ARC irrespective of genetic background.**
234
235 To understand the role of *afu-182* in fungal ARC, we tested the RNA levels of *afu-182* in the
236 presence and absence of azoles. A significant reduction in levels of *afu-182* was observed
237 in strains grown in the presence of either voriconazole or posaconazole compared to GMM
238 (Figure 5A). Multiple strains of *A. fumigatus,* including A1163, CEA10 and Af293, are used
239 as laboratory WT strains (44). Additionally, multiple reports have shown significant strain
240 virulence heterogeneity, thus making it hard to establish a true WT strain (45); however, a
241 comprehensive study of azole response in ASAF strains is lacking. To further determine the
242 role of *afu-182* in regulating fungal ARC, we quantified the relative abundance of *afu-182*
243 RNA levels in CEA10, Af293 and an environmental isolate 47-57. Interestingly, *afu-182* RNA
244 levels negatively correlate with fungal ARC irrespective of MIC (Figures S3E-S3F). The Af293
245 strain is inherently more recalcitrant to voriconazole (Figure S3F). We made a Δ*afu-182*
246 mutant in the Af293.1 background, and the resulting strain showed increased fungal ARC at
247 0.4μg/ml (compared to 0.25μg/ml for CEA10) due to inherent differences in azole response
248 between strains (Figures 5B and 5D). Environmental isolate 47-57 has increased RNA levels

249 of *afu-182* compared to CEA10 and is more susceptible to voriconazole compared to
250 CEA10 (Figures S3E and S3F). Deletion of *afu-182* in the 47-57 background also resulted in
251 increased fungal ARC at 0.1μg/ml (Figures 5C and 5E). These two isolates with azole
252 sensitivity on either side of CEA10 showed increased fungal ARC upon *afu-182* loss,
253 highlighting the role of *afu-182* irrespective of the strain's background. To further
254 characterize the role of *afu-182* in fungal ARC, we identified the *afu-182* homolog in the
255 related species *A. nidulans*. The deletion of *an-182* (Δ*an-182*) in two distinct AN isolates
256 (A1145 and GR5) also leads to fungal ARC (Figures 5F and 5G), indicating roles of lncRNA
257 *afu*-182 homologs in multiple Aspergilli species.
258
259 ***afu-182* does not affect azole-regulating transcription factors *srbA*, *atrR* or azole target**
260 **gene *cyp51* (erg11a and erg11b)**
261
262 To further test the role *of afu-182* in regulating ARC, we quantified the mRNA levels of azole
263 target genes *cyp51a* and *cyp51b,* both in the presence and absence of azoles and TFs *srbA*
264 and *atrR* in GMM. Importantly, we did not see a change in the transcript levels of *cyp51*
265 genes in the absence of azoles (Figures 6A and 6B). While in the presence of azoles, we
266 clearly see an upregulation of *cyp51a* based on drug response, no upregulation was seen
267 due to genotype (Two-Way ANOVA, interaction p-value = 0.3291, Figure 6A). We did see an
268 interaction between genotype and drug response for *cyp51b* (Two-way ANOVA, interaction
269 p value = 0.0045), but post-hoc analysis showed no difference between WT and Δ*afu-182*
270 strains in either condition (p = 0.2171 for GMM and p = 0.9163 for GMM + vori, Figure 6B).
271 We also did not see a change in mRNA levels of transcription factors, *srbA* and *atrR*, that
272 are mainly associated with *cyp51a/b* expression (Figures 6C and 6D). We also did not see a
273 change in *insA* mRNA levels (Figure 6E). Thus, *afu-182* and fungal ARC represent a distinct
274 mechanism of fungal response to azole drugs that is independent of azole target gene
275 transcript levels.
276
277 ***afu-182* regulates the RTA family of proteins:**

To determine the role of *afu-182* in regulating fungal ARC, we used a global transcriptomic approach. Interestingly, we determined that the transcript levels of the RTA1 family of genes are increased in the presence of azoles in WT strains. The RTA1 family encodes a diverse family of proteins with wide-ranging functions. In *Saccharomyces cerevisiae*, members of this family are involved in resistance to 7-aminocholestrol (RTA), resistance to molasses (RTM), and lipid and heme transport (46). Previous reports have suggested that a member of the RTA1 family is the most increased transcript in response to itraconazole in clinical samples (47). In *A. fumigatus*, we identified 23 genes encoding RTA1 family proteins. Interestingly, most of these genes are expressed at very low RNA levels (FPKM <5 for 17 genes in the glucose minimal medium conditions examined). We selected 12 genes that showed significant increases in transcript levels and have an FPKM value >1 and performed qPCR to compare their mRNA levels in the presence and absence of azoles. All 12 gene transcripts were increased in the presence of azoles (Figure 7).

To further understand the role of *afu-182* mediated ARC and its relationship to RTA1 family of proteins, we plotted volcano plots of significant genes ($-2<\log_2>2$) between WT GMM vs WT azole, WT azole vs Δ*afu-182* azole, Δ*afu-182* GMM vs Δ*afu-182* azole, and WT azole vs comp-182 azole (Figures 8 A-D). We observed that the transcripts of two genes *afub_000050 and afub_000060* were significantly increased in the presence of azoles in the WT strain and the Δ*afu-182* strain (Figures 8A and 8B). Transcripts of both these genes were further increased in the Δ*afu-182* strain compared to the WT in the presence of azoles, hinting at negative regulation of these genes by *afu-182* (Figure 8C) and did not show differential regulation in the comp-182 strain compared to the WT (Figure 8D). We confirmed this expression pattern with qPCR (Figures 8E and 8F). Both *afub_000050* and *afub_000060* showed a significant interaction between genotype and azole response (Two-Way Anova, $p<0.0001$). Of the 23 genes in the RTA1 class, these two are annotated as RTM1 proteins, a homolog of the *S. cerevisiae* gene providing resistance to molasses (48). We termed them as *rtmA* and *rtmB,* respectively. These genes are present next to each other in the genome and are divergently expressed.

307 ***rtmA* and *rtmB* are sufficient in driving fungal ARC:**

308

309 To ascertain the role of *rtmA* and *rtmB* in fungal ARC, we deleted them in the CEA10
310 background. Additionally, we made a double null mutant Δ*rtmA*Δ*rtmB* strains. We also
311 ectopically complemented *rtmA* and *rtmB* single mutants. Both the Δ*rtmA* (31% decrease
312 in growth ratio, p=0.0012 One-Way ANOVA) and Δ*rtmB* (42% decrease in growth ratio,
313 p<0.0001, One-Way ANOVA) strain showed reduced fungal ARC in response to azole drugs
314 (Figure 9A-B, and 9C-D), whereas the Δ*rtmA*Δ*rtmB* strain also showed significant growth
315 attenuation in presence of azoles (46% decrease in growth ratio p<0.001, One-Way
316 ANOVA), indicating a combined role of these genes in regulating fungal azole response,
317 where *rtmB* is the major driver of the ARC phenotype (9E and 9F). The complement strains
318 reverted to the WT levels, indicating a causal role of these genes in fungal ARC (Figures 9A-
319 9D, inset – macro lens images). Our RNA analysis revealed that comp strains have 4-6-fold
320 increases in *rtmA* and *rtmB* expression in these strains compared to WT in the presence of
321 azoles (Figures S4A-B). As the FPKM values are <5 for these genes in GMM, we chose to test
322 the RNA levels under stress conditions. Further studies are needed to determine the
323 functional redundancy of other genes in this family; however, recently, an RTA1 family
324 protein, *rtaA,* was shown to play no role in azole response (49). The functions of these
325 genes appear to be diverse.

326

327 **Discussion:**

328

329 While increasing azole resistance in *A. fumigatus* is a major concern, azole-
330 susceptible strains (ASAF) still cause most infections. Crucially, the inherent rise of drug
331 resistance in 43% of patients could not be attributed to changes in the *cyp51A* sequence
332 (50), the major driver of fungal resistance caused by agricultural use of azoles (51). This
333 hints at a broader response to AF drugs, especially in ASAF, during infections. Here, we
334 show that the long non-coding RNA *afu-182* negatively regulates fungal response to azole
335 drugs in ASAF isolates (Figures 2 and 3). Importantly, deletion of *afu-182* is not associated

336 with a change in MIC (Figure S3B); however, the Δ*afu-182* strain grows more in the presence
337 of sub-MIC levels of azole drugs, a phenomenon we term here as fungal ARC (Figures 2 and
338 3). Fungal response to drugs has been characterized based on changes in genetic
339 sequence (i.e., resistance) or non-genetic mechanisms (tolerance, persistence, and
340 hetero-resistance) (29, 30). For bacterial populations, tolerance is defined as increased
341 survival in the presence of antibiotic concentrations above MIC without a change in MIC
342 (52). For molds, tolerance is defined as the ability of the fungal strain to grow in the
343 presence of anti-fungal drugs above the MIC, and the definition is further refined to
344 tolerance as a property against fungistatic drugs (30, 31). Here, we showed that deletion of
345 *afu-182* did not change the MIC for azoles. Azoles have been shown to induce cell wall
346 carbohydrate patches to kill AF (53). As alluded to before, *Aspergillus* strains differ in their
347 stress responses and virulence (45), and because drug MICs also differ amongst strains, it
348 is hard to predict if azoles are killing AF (i.e., fungicidal) at the MIC or above the MIC. For
349 example, cell wall patches, a sign of fungicidal activity, were induced in the AfS35 strain
350 (53) using drug concentrations above MIC (53, 54). Similarly, azole persistence was shown
351 as cells growing in the zone of inhibition in a disk-diffusion assay (31) and defined as the
352 ability of a small fraction of cells to grow at drug concentrations above the MIC of fungicidal
353 drugs (30). However, we did not see the presence of persister colonies in Δ*afu-182* strains
354 in the E-test assay (Figure 3H) and did not see fungal growth at 2x MIC. Thus, we defined the
355 Δ*afu-182*-mediated phenotype as ARC, a distinct response from tolerance and persistence.
356 Furthermore, we showed that the Δ*afu-182*-mediated ARC phenotype is independent of the
357 strain's background and is conserved in *A. nidulans* and is a fungal response measured at
358 0.5x MIC azole concentration.
359 We also showed the azole recalcitrance of surface-attached AF, classically defined
360 as biofilms (55). Drug resistance is a classical feature of the biofilms (56), and even though
361 we saw increased attached fungal biomass for the Δ*afu-182* strain upon azole treatment
362 (Figure 2C), it is possible that different mechanisms are playing roles in this distinct growth
363 conditions. For example, metabolic adaptation, drug binding to the ECM, and oxygen
364 gradients have all been shown to play a role in biofilm mediated drug resistance.

365 Additionally, biofilms can lead to persister cells (57). Further research will uncover the role
366 of fungal ARC in surface biofilm (as on agar plate) vs. submerged biofilms.
367 The intergenic lncRNA *afu-182* is located next to the *insA* gene, which was recently
368 shown to regulate the fungal response to azole drugs. The INSIG homolog, *insA*, regulates
369 HMG-CoA as the basis of azole resistance (28), but we did not see a change in the mRNA
370 levels of *insA* in the Δ*afu-182* strains (Figure 6). Trans-acting over-expression of the *afu-182*
371 (OE-182) also resulted in decreased fungal growth in the presence of azoles, suggesting an
372 *insA* transcription-independent mechanism (Figures 2 and 3); however, post-
373 transcriptional or translation regulation of *insA* is still possible and might play a role in ARC.
374 Future research will uncover the basis of *afu-182* regulation.
375 Different AF isolates show differential *afu-182* regulation, implying that *afu-182*
376 might be involved in fungal adaptation to stress, though in our murine model, it was not
377 required for virulence (Figure 4 and S3E). Thus, the evolutionary significance of *afu-182* in
378 AF is currently unclear. Importantly, the Δ*afu-182* strain shows fungal ARC only in response
379 to azole stress and does not play a role in response to the polyene and echinocandin
380 classes of drugs (data not shown). Over 90% of infections are still caused by ASAF, with
381 treatment failure rates approaching 50-90% (58, 59). It is imperative to better understand
382 the fungal response to azole drugs. To understand the role of *afu-182* in fungal response *in*
383 *vivo*, we used a steroid model of IPA. In the absence of azole drugs, the Δ*afu-182* strain is
384 pathogenic and equally virulent as WT (Figure 4B); however, in the presence of 5mg/kg of
385 posaconazole, our data show increased virulence in the Δ*afu-182* strain as measured by
386 survival analysis and fungal burden analysis (Figure 4E and 4H). The overexpression strain
387 did not show a change in survival compared to WT when treated with azole drugs (Figure
388 4E); however, it showed a 90% reduction in fungal burden, highlighting the role of *afu-182* in
389 virulence (Figure 4H). In a steroid model of invasive aspergillosis, deaths due to
390 exacerbated immune response have been reported (59), and it is plausible that this is the
391 case in OE-182-infected azole-treated animals. In vitro, we see that *afu-182* regulates pan-
392 azole ARC, including to posaconazole (Figure 3D).

393 Different isolates of *A. fumigatus* have been previously shown to differ in virulence.
394 Some of the factors attributed to this difference are nutrient plasticity and response to light
395 and oxygen (60–62); however, how different azole-susceptible isolates respond to azole
396 drugs and their virulence potential in relation to azole treatment requires further research.
397 *afu-182* regulates fungal ARC in ASAF irrespective of the strain's background, as indicated
398 by deletion of *afu-182* in the laboratory isolates CEA10 and Af293 backgrounds (44).
399 Additionally, deletion of *afu-182* in the environmental isolate 47-57 also leads to ARC
400 (Figure 5B and 5C) (60).
401 The emergence of new strains provides a unique challenge in studying *Aspergillus*
402 pathogenicity, but *afu-182* appears to play a role irrespective of the strain's background.
403 One possible reason for this might be the mechanisms by which ncRNA functions. LncRNA
404 may provide stress adaptation in the absence of evolution that is associated with genomic
405 changes (63). A rapid adaptation will increase the likelihood of fungal survival during stress,
406 leading to DNA change. A recent study identified 1089 novel long non-coding RNAs; eleven
407 of which negatively regulate fungal response to azole drugs; however, *afu-182* fell below the
408 size threshold identified in this study (64). How *afu-182* regulates fungal ARC is not yet
409 clear. As the RNA levels of transcription factors involved in azole resistance, viz., *srbA*, *atrR*
410 and azole target genes *cyp51a* and *cyp51b,* are not impacted by *afu-182* (Figure 6), *afu-182*
411 regulates fungal ARC through a novel mechanism.
412 As long non-coding RNAs function in diverse ways, we used a transcriptomic
413 approach to identify the genes directly or indirectly regulated by *afu-182* at the RNA levels.
414 In the presence of azoles, we see the RTA1 family of proteins upregulated in WT (Figure 7).
415 This is a 7-transmembrane domain family of proteins and has been associated with lipid
416 and heme export and resistance to 7-amonicholesterol in *S. cerevisiae* and *Cryptococcus*
417 *neoformans* (46, 65) and consists of 23 members in *A. fumigatus*. Recently, *rtaA*
418 (Afu3g12830, CEA10 homolog - *afub_036340*) was shown to play a role in response to the
419 polyene class of drug, amphotericin B and not azoles (49). Here, we identified *rtmA* and
420 *rtmB* (Figure 8A-C), two divergent genes downstream of *afu-182*, situated next to each other
421 to regulate fungal ARC (Figure 9). Both *rtmA* and *rtmB* are negatively regulated by *afu-182*

422 (Figures 8 B and C); however, *rtmB* mutations might be epistatic to mutations in *rtmA,* as
423 the double deletion strains show nearly the same inhibition as Δ*rtmB* (Figures 9 D and F).
424 As both these genes are next to each other, it is not clear whether *afu-182*, by itself or in
425 coordination with other complex members, if any, regulates the promoter region of these
426 genes. It is also possible that these genes evolved due to a duplication event to maintain
427 tight regulation for xenobiotic stress. If *afu-182* regulates fungal ARC via direct regulation of
428 RTM/RTA1 domain-containing proteins is an active and ongoing area of research in the
429 laboratory. Importantly, *rtmA* and *rtmB* belong to the accessory genome of AF and were
430 detected in only 7 of the 300 genomes analyzed (66). In *S. cerevisiae,* RTM1p was also
431 absent from laboratory strains (48). Given that there are twenty-three members of the same
432 class of proteins, it is possible that gene duplication added more members in some strains
433 of AF. The functional redundancy in other strains would still allow *afu-182*-mediated RTA1-
434 dependent fungal ARC morphology. This genetic diversity and gene duplications in AF
435 strains have been previously reported (67). More research will uncover the function of this
436 family of proteins in the future.
437 Long non-coding RNAs mainly function through their secondary structure and are
438 difficult to predict based on the nucleotide sequence alone (68). Here, using synteny, we
439 identified *afu-182* homolog in related fungal species *A. nidulans*. Deletion of *afu-182*
440 homolog, *an-182,* also leads to fungal ARC in *A. nidulans,* showing its role in regulating
441 azole response in multiple Aspergilli (Figures 5F and 5G). Whether *afu-182* homologs play a
442 role in the phytopathogens *A. flavus* and *A. parasiticus* is unknown and needs more
443 research; complex approaches are needed to identify the homologs of *afu-182* in other
444 fungal pathogens. However, our data clearly show that long non-coding RNA, *afu-182,*
445 regulates fungal ARC in AF and AN irrespective of the strain's background.
446 In conclusion, the lncRNA *afu-182* regulates fungal response to azole drugs in both
447 ASAF and the related fungal species AN. This effect, in ASAF, is at least partially driven via
448 negative regulation of *rtmA* and *rtmB*. As MIC is a poor predictor of azole treatment
449 outcomes in ASAF strains, further characterization of *afu-182* levels will help us determine

450 the fungal response to azole drugs *in vivo*. Given advancements in RNA biology, *afu-182*
451 also presents a target to augment the efficacy of current azole drugs.
452
453 **Materials and Methods**
454
455 **Fungal strains**
456 *Aspergillus fumigatus* (AF) strain CEA10 or CEA17 was used as the host strain to generate
457 subsequent strains. For *A. nidulans*, A1145 (FGSC) and GR5 (FGSC) were used as the host
458 strains to generate subsequent strains. For *A. nidulans*, the strains were supplemented
459 with Uridine (1.26g/L), Uracil (0.56g/L), pyridoxine (0.05μg/ml), p-amino-benzoic acid
460 (PABA) (5μM) and riboflavin (0.1μg/ml). All experiments with stationary fungal growth were
461 performed at 37°C in the presence of 5% CO_2. Liquid biomass and germination assay were
462 performed in the absence of supplied CO_2. All strains were stored as 30% glycerol stocks in
463 -70°C for long-term storage. The list of strains used and generated is listed in Supplemental
464 Table 1.
465
466 **Δ*insA* strain construction:**
467 The *insA* deletion strain was created using homologous recombination. Fusion PCR was
468 used to create the DNA deletion cassette. Briefly, the 5' and 3' fragments of *insA* were
469 amplified with primers RAC 815 and RAC 816, and RAC819 and RAC820, respectively. A
470 gene encoding for *pyrG* was amplified from pJW24 (69) using primers RAC817 and RAC818.
471 The three fragments were fused together using primers RAC 821 and RAC 822. The resulting
472 DNA fragment was transformed into the CEA17 strain via PPEG-mediated transformation of
473 protoplast (70). Strains were checked with PCR, Southern blot for single integration and
474 qPCR for lack of detectable RNA. This strain does express *afu-182* at the native locus.
475
476 **Complementation plasmid construction**: A plasmid encoding for *pyrithiamine*
477 resistance, BS309, was created as follows. Two oligo fragments (SD37 and SD38) encoding
478 for 5' SacI overhang-AscI-BglII-MluI-Pac1-SacII-3' overhang were ordered from IDT and

479 were allowed to anneal in the thermocycler. The resulting dsDNA fragment with SacI-SacII
480 overhangs was ligated into pBS KS (+) plasmid previously digested with SacI and SacII,
481 resulting in plasmid BS309 intermediate. A DNA fragment encoding for pyrithiamine
482 resistance was amplified from pSD51 with primers RAC3280 and RAC3154 expressing an
483 XhoI restriction site (71). The DNA fragment was digested with XhoI and ligated into BS309
484 intermediate previously digested with SalI, resulting in the plasmid BS309.
485
486 **Plasmid construction for Comp-*insA* with cis acting *afu-182***: A DNA fragment consisting
487 of ~1kb 5' region of *insA* along with *insA* and 485bp after the transcription end site (as
488 determined by RACE) expressing AscI and PacI restriction sites at the 5' and 3' ends,
489 respectively, was amplified with primers RAC3589 and RAC3591 using Takara Prime Star
490 HS polymerase per manufacturer's recommendation. The resulting DNA fragment was
491 digested with AscI-Pac1 and was ligated into BS309, resulting in comp-cis *insA* plasmid.
492
493 **Plasmid Construction for Comp-*insA* without cis-acting *afu-182***: A DNA fragment
494 consisting of 5' region of *insA* along with *insA* and 74bp after the transcription end site
495 (without ncRNA *afu-182*) expressing AscI and PacI restriction sites at 5' and 3' ends
496 respectively, was amplified with primers RAC3589 and RAC3590 using Takara Prime Star
497 HS polymerase per manufacturer's recommendation. The resulting DNA fragment was
498 digested with AscI-Pac1 and was ligated into BS309, resulting in comp-without cis-182 *insA*
499 plasmid.
500
501 The resulting plasmids were transformed into the Δ*insA* strain using PEG-mediated
502 transformation of protoplast as previously described (70).
503
504 **Δ*afu-182* strain construction**: *afu-182* was deleted from the strain CEA17 (*pyrG*-) using
505 CRISPR-Cas9 as previously described (72). A homology-directed repair cassette was
506 amplified from plasmid pSD38.1 using primers SD149_182 homology F and SD150_182
507 homology. Briefly, 5µl of 100mM crRNAs (on either side of *afu-182*) were combined with 5µl

508 of 100mM tracrRNA and 5 µl of nuclease-free duplex buffer (IDT), heated to 95°C for 5 min
509 and allowed to cool to room temperature, yielding 33mM gRNA complex. Then, 1.5 µl of
510 each guide RNA complex on either side of *afu-182* were combined with 1.5µl of Cas9
511 (1mg/ml) and 22µl of Cas9 working buffer as previously described (72). The samples were
512 allowed to combine at RT for 5 min to allow the assembly of the RNP complex. RNP
513 complex and repair cassette were transformed via PEG-mediated transformation of the
514 CEA17 strain as previously described (70, 72). The same gRNAs and HDR were also used to
515 delete *afu-182* in the Af293.1 strain and 47-7 strain (60). The sequence of crRNAs and
516 primers used is provided in Tables S2 and S3.
517
518 **Comp-182 strain construction**: *afu-182* was put back at its genomic location using
519 CRISPR-Cas9. Briefly, the *afu-182* fragment was amplified with primers SD76 and 164 using
520 CEA10 gDNA as template. A gene encoding for pyrithiamine resistance was amplified from
521 plasmid pSD51.1 (71) using primers SD23 and SD165. Both fragments were fused using
522 primers SD183 and SD166, generating the HDR cassette. A single gRNA (gRNA 13 SD 1)
523 targeting the linker sequence in the *pyrG* gene was used for double-strand break, and HDR
524 was used to insert *afu-182* back at the locus.
525
526 **OE *afu-182*pyrG plasmid construction**. The *A. nidulans gpdA* promoter was amplified
527 from strain FGSC A4 (FGSC) using primers SD134 and SD103. The *afu-182* fragment was
528 amplified from CEA10 gDNA using primers SD104 and SD105. Subsequently, these
529 fragments were fused using primers SD135_EcoRI and SD139_NotI and digested with
530 EcoRI and NotI. The resulting fragment ligated into plasmid pSD21 previously digested with
531 EcoR1 and Not1, yielding plasmid OE*afu-182*pyrG. The *afu-182* RNA expression starts at the
532 +1 transcription start site (TSS).
533
534 **CEA10 OE *afu-182* strain construction**: CRISPR-Cas9 was used to target the OE *afu-182*
535 *pyrG* HDR cassette to the safe-haven *atf4* locus (73) as previously described (64). The HDR
536 was amplified from plasmid OE *afu-182pyrG* using primers SD162_OE_homology-F and

537 SD163_OE_homology-R. gRNA was assembled as described above for the Δ*afu-182* strain.
538 A single guide (atf4_gRNA7) was used to initiate a double-stranded break targeting the *atf4*
539 locus (73).
540
541 Polyethylene glycol-mediated fungal transformation was done as described above. All
542 resulting transformants were checked with PCR and confirmed with Southern blot and
543 qPCR for gene expression.
544
545 ***Aspergillus nidulans* Δ*182* (Δ*an-182*) construction.**
546 A DNA sequence homologous to *afu-182* was identified 240bp after the translational stop
547 site of the *insA* homolog gene AN4465 (34). The resulting 200bp sequence was deleted
548 from the *A. nidulans* genome using CRISPR-Cas9 in the A1145 strain using the *pyrG* marker
549 or the GR5 strain using the *pyroA* marker as previously described (72). The HDR cassette for
550 A1145 was amplified using primers SD181 and SD182 that amplified the sequence of
551 orotidine 5'-phosphate decarboxylase (74) gene from *A. parasiticus* using plasmid pSD38.1
552 (75) as template. The HDR cassette for GR5 was amplified with SD 352 and SD 353, which
553 amplified the pyridoxine biosynthesis gene (76) from *A. fumigatus* using CEA10 as the DNA
554 template.
555
556 **Δ*rtmA*, Δ*rtmB and* Δ*rtmA*Δ*rtmB* strains construction:**
557
558 Δ*rtmA* and Δ*rtmB* strains were constructed using the CRISPR-Cas9 protocol as previously
559 described for the Δ*afu-182 strain* (64). The HDR cassette primers and crRNA sequences are
560 provided in Table S1. Δ*rtmA* and Δ*rtmB* strains were constructed in the CEA10 background
561 using the pyrithiamine resistance marker, *ptrA* from pSD51.1. For Δ*rtmA*, crRNA 50L and
562 50R were used, for Δ*rtmB*, crRNA 60L and 60R were used. For double deletion strains,
563 crRNAs 60R and 50R were used. HDRs were amplified using primers SD151 and SD152 for
564 Δ*rtmA* deletion; SD153 and SD154 for Δ*rtmB* deletion and primers SD152 and SD153 for
565 double deletion.

566 **Complement *rtmA* and complement *rtmB* strain construction:**

567

568 Hygromycin resistance gene expressing plasmid: Hyg resistance gene was amplified using
569 the primers RAC2939 and RAC2940 from the plasmid pBC Hygro (FGSC) and was ligated
570 into pJET1.2 (Thermo Fisher). The fragment was digested using XhoI-XbaI and was ligated
571 into the plasmid BS309 (see above), previously digested with XhoI and XbaI, resulting in
572 plasmid BS311.

573

574 **Plasmid construction for Comp *rtmA* strain:** The *rtmA* fragment, along with the promoter
575 and terminator region, was amplified (CEA10 gDNA template) using the primers SD738 and
576 SD739 with Asc1 and Pac1 restriction sites, respectively, using NEB Q5 hot start
577 polymerase per manufacturer's recommendation. The resulting DNA fragment was
578 digested with AscI and PacI and was ligated into the plasmid BS311 previously digested
579 with AscI and PacI, resulting in the Comp-*rtmA* plasmid.

580

581 **Plasmid construction for comp-*rtmB* strain:** The *rtmB* fragment, along with the promoter
582 and terminator regions, was amplified (CEA10 gDNA template) using the primers SD740
583 and SD741 with Asc1 and Pac1 sites, respectively, using NEB Q5 hot start polymerase per
584 manufacturer's recommendation. The resulting DNA fragment was digested with AscI and
585 PacI and was ligated into BS311 previously digested with AscI and PacI, resulting in the
586 Comp-*rtmB* plasmid.

587

588 Comp-*rtmA* and comp-*rtmB* plasmids were transformed into Δ*rtmA* and Δ*rtmB* strains,
589 respectively, as described above.

590

591 **Spot assays:**

592

593 Plates containing solid GMM were spot inoculated with serially diluted AF spores (10^5-10^2
594 spores) and grown at 37°C as indicated. Azole drugs were used at the indicated

595 concentrations for MIC assays and 0.5 X MIC for ARC assays. The radial diameter of the
596 colonies was measured and reported as the growth ratio, dividing the colony radial
597 diameter in the presence of azole by the colony radial diameter in GMM. All experiments
598 were done at least in triplicate and were repeated three times. Statistical analyses (t-test or
599 one-way ANOVA) were done to determine the significant differences using GraphPad
600 Prism.
601
602 **Biomass assay:**
603
604 Spores were grown in 50 ml liquid GMM (1 x 10^6 spores/ml) at 37°C for 24 hours in the
605 presence or absence of 0.2 µg/ml voriconazole with continuous shaking at 250rpm.
606 Mycelium collected after 24 hours was lyophilized, and the biomass was weighed.
607 Statistical difference between means was assessed with One-way ANOVA followed by
608 Tukey's post hoc analysis to compare individual groups using GraphPad Prism.
609
610 **Biofilm formation assay:**
611
612 AF spore suspension (1.5 x 10^5 spores/ml) in liquid GMM was inoculated in three biological
613 replicates in a 12-well plate. The plates were centrifuged at 250g for 10 min to settle the
614 conidia at the bottom of the wells and incubated at 37°C for 12 hours. Then, the wells were
615 washed twice with PBS to remove planktonic cells. The biofilms at the bottom of the wells
616 were further allowed to grow in the presence of 0.2 µg/ml Voriconazole for 8 hours before
617 the crystal violet assay was performed as previously described (37). Absorbance was
618 measured using a plate reader (Multiscan Sky, Thermo Scientific) at 600 nm. All
619 experiments were done in triplicate, and three independent experiments were performed.
620 Statistical significance was determined with One-way ANOVA using GraphPad Prism.
621
622 **Germination assay:**
623

624 AF spores ($2x10^4$/ml) collected from 48-hour-old colonies grown in GMM were inoculated in
625 a 96-well plate (six replicates per strain) in liquid GMM (no drug) and GMM containing 0.2
626 μg/ml voriconazole. Absorbance (OD_{600}) was measured in a plate reader every 15 minutes
627 at 37°C for 12 hours. The experiment was repeated three times. Statistical significance was
628 determined with one-way ANOVA using GraphPad Prism.
629
630 **E-test assay:**
631
632 Five milliliters of GMM top-agar (0.75%) containing AF spores ($1x\ 10^5$/5 ml) were spread on
633 GMM plates and allowed to solidify. A voriconazole E-test strip (Biomerieux) was carefully
634 laid in the center of the plate per the manufacturer's recommendation. The plates were
635 incubated at 37°C for 48 hours, and the minimum inhibitory concentration (MIC) was
636 recorded. The experiment was done in triplicate for each strain and repeated three times.
637
638 **Broth Microdilution assay:**
639
640 AF spores (5×10^4) collected from a 48-hour-old colony were inoculated in liquid GMM in a
641 96-well plate containing voriconazole (16μg/ml – 0.015μg/ml) and incubated at 37°C for 48
642 hours. The visible growth of AF strains was observed in each of the wells, and the lowest
643 concentration of azoles showing no growth for an AF strain was recorded as MIC. The
644 experiment was repeated three times.
645
646 **Murine model of pulmonary aspergillosis, lung histopathology, and fungal burden:**
647
648 Outbred female CD-1 mice (Charles River Laboratories) with body weights of 18-21 g were
649 housed (5 per cage) in micro-isolator cages. The mice were kept in a soft-lit, well-ventilated
650 cubicle with a 12h:12h light/dark cycle. Mice were immunosuppressed with a single
651 subcutaneous injection of 40 mg/kg body weight of Triamcinolone acetonide (Kenalog-10,
652 Bristol-Myers Squibb) on day -1. Mice were briefly anesthetized with isoflurane and infected

653 by intranasal instillation of 2 x 10^6 spores in 40μL PBS. Ten mice were infected per AF strain
654 for survival analysis, whereas five mice per strain were used for fungal burden analysis. The
655 mice were observed for 14 days for their survival. For azole treatment, 5 mg/kg
656 Posaconazole (Noxafil, oral suspension, Merck) diluted in PBS was used.
657
658 For fungal burden analyses, mice were treated with 5 mg/kg Posaconazole on day +1 and
659 day +2, and their lungs were harvested on day +3. The mouse lungs were lyophilized
660 overnight, homogenized with 2.3 zirconia beads, and lysed with LETS buffer (0.1M LiCl,
661 10mM EDTA pH 8.0, 10mM Tris-Cl pH 8.0, 0.5% SDS). Total DNA was extracted in an
662 aqueous phase using phenol: chloroform: isoamyl alcohol and precipitated with
663 isopropanol. Fungal burden was determined by calculating the levels of 18s rRNA encoding
664 gene against a standard curve using iTaq universal probe mix and hydrolysis probe as
665 previously described (42). The statistical significance of survival analysis was determined
666 using log-rank analysis, and fungal burden analysis was done using a non-parametric
667 Mann-Whitney U Test.
668
669 For histological analysis, lungs were harvested from untreated mice on day +3 and were
670 fixed in 10% formalin for 48 hours before microdissection at the Clemson Light Imaging
671 Facility (CLIF) at Clemson University. Adjacent slides obtained from microdissection were
672 stained with Grocott's Methenamine Silver and Hematoxylin and Eosin stains as previously
673 described (41). The stained slides were pictured with the Leica Laser Microdissection
674 Microscopy System at CLIF.
675
676 **RNA extraction:**
677
678 For RNA sequencing, total RNA was extracted from AF strains CEA10, Δ*afu-182*, comp-182,
679 and OE-182 strains. Briefly, 1 x 10^4 spores were spot inoculated and incubated at 37°C for
680 48 hours on solid GMM plates in the absence or presence of voriconazole (0.15 μg/ml). The
681 whole colonies from samples were excised with a clean scalpel and flash frozen in liquid

682 N_2. The frozen samples were homogenized with 2.3 mm zirconia beads in acid guanidinium
683 thiocyanate phenol, and RNA was extracted using the acid guanidinium thiocyanate phenol
684 chloroform (AGPC) method as described with some modifications (77). Briefly, the
685 aqueous phase was mixed with ethanol to a final concentration of 35%. The resulting mix
686 was passed through RNA-binding columns (Epoch Life Sciences), washed twice with 70%
687 Ethanol and eluted in nuclease-free water. The RNA was treated with Turbo DNase (Thermo
688 Fisher) per the manufacturer's recommendation and purified using magnetic beads
689 (Beckman Coulter). RNA quantity and quality were estimated using the AccuBlue Broad
690 Range RNA Quantitation Kit (Biotium) and the Quantum Fluorometer (Promega), and via gel
691 electrophoresis, respectively, before submission of the samples to LC Sciences.
692 Sample quality was checked by Agilent Technologies 2100 Bioanalyzer at LC Sciences. The
693 poly(A) RNA sequencing library was prepared following Illumina's TruSeq-stranded-mRNA
694 sample preparation protocol. Poly(A) tail-containing mRNAs were purified using oligo-(dT)
695 magnetic beads with two rounds of purification. After purification, poly(A) RNA was
696 fragmented using a divalent cation buffer at elevated temperature. Quality control analysis
697 and quantification of the sequencing library were performed using Agilent Technologies
698 2100 Bioanalyzer High Sensitivity DNA Chip. Paired-end sequencing was performed on
699 Illumina's NovaSeq 6000 sequencing system.
700
701 **RNA-seq analyses**
702
703 Transcript expression was determined by first aligning RNA-Seq reads to the *A. fumigatus*
704 A1163 genome obtained from FungiDB v68 (34) with the splice-aware aligner STAR
705 v2.7.11a (78). The resulting SAM file for each experimental replicate was processed with
706 samtools v1.19.2 (79) and featureCount v2.0.6 (80) to produce a table of read counts per
707 annotated gene locus. The read counts were analyzed with DESeq v1.46.0 (81) and plotted
708 with EnhancedVolcano v1.24.0 (82) in the R v4.4.2 statistical environment(83). The pipeline
709 for analyzing these is archived in a GitHub repository
710 (https://github.com/stajichlab/DhingraLab_ncRNA_Afumigatus) and Zenodo (84)

711 **Assessment of gene expression by RT-qPCR**
712

713 For qPCR, 48-hour-old AF colonies grown at 37°C in solid GMM plates with or without
714 voriconazole (0.15μg/ml) were extracted as described above. RNA samples were then
715 treated with Turbo DNase per the manufacturer's recommendations. Equal amounts of
716 DNase-treated RNA were used for first-strand cDNA synthesis using MMLV reverse
717 transcriptase (Promega) per the manufacturer's recommendation. Quantitative PCR (CFX
718 real-time PCR system - Bio-Rad) was done using the sso Advanced universal SYBR green
719 supermix (Bio-Rad). Histone H4 was used as the reference gene for normalization. All
720 primers used in the study are listed in Supplementary Table 2.
721

722 **<u>Data Availability:</u>**
723

724 The RNA-seq sequencing data and per-gene read counts are available from Sequence Read
725 Archive associated to BioProject PRJNA1334547 and in Gene Expression Omnibus under
726 accession GSE309441.
727

728 **Statistical analyses**
729 GraphPad Prism 10 for macOS was used to perform all statistical analyses.

730 **References:**
731

732 1. Morrissey CO, Kim HY, Duong T-MN, Moran E, Alastruey-Izquierdo A, Denning DW,
733 Perfect JR, Nucci M, Chakrabarti A, Rickerts V, Chiller TM, Wahyuningsih R, Hamers
734 RL, Cassini A, Gigante V, Sati H, Alffenaar J-W, Beardsley J. 2024. Aspergillus
735 fumigatus—a systematic review to inform the World Health Organization priority list of
736 fungal pathogens. Med Mycol 62:myad129.

737 2. Baddley JW. 2011. Clinical risk factors for invasive aspergillosis. Med Mycol 49 Suppl
738 1:S7–S12.

739 3. Latgé J-P, Chamilos G. 2019. Aspergillus fumigatus and Aspergillosis in 2019. Clin
740 Microbiol Rev 33:e00140-18.

741 4. Liu K-W, Grau MS, Jones JT, Wang X, Vesely EM, James MR, Gutierrez-Perez C, Cramer
742 RA, Obar JJ. 2022. Postinfluenza Environment Reduces Aspergillus fumigatus
743 Conidium Clearance and Facilitates Invasive Aspergillosis In Vivo. mBio 13:e02854-
744 22.

745 5. Sarden N, Sinha S, Potts KG, Pernet E, Hiroki CH, Hassanabad MF, Nguyen AP, Lou Y,
746 Farias R, Winston BW, Bromley A, Snarr BD, Zucoloto AZ, Andonegui G, Muruve DA,
747 McDonald B, Sheppard DC, Mahoney DJ, Divangahi M, Rosin N, Biernaskie J, Yipp BG.
748 2022. A B1a–natural IgG–neutrophil axis is impaired in viral- and steroid-associated
749 aspergillosis. Science Translational Medicine 14:eabq6682.

750 6. Tio SY, Chen SC-A, Hamilton K, Heath CH, Pradhan A, Morris AJ, Korman TM, Morrissey
751 O, Halliday CL, Kidd S, Spelman T, Brell N, McMullan B, Clark JE, Mitsakos K, Hardiman
752 RP, Williams P, Campbell AJ, Beardsley J, Van Hal S, Yong MK, Worth LJ, Slavin MA.
753 2023. Invasive aspergillosis in adult patients in Australia and New Zealand: 2017–
754 2020. The Lancet Regional Health - Western Pacific 40:100888.

755 7. WHO fungal priority pathogens list to guide research, development and public health
756 action. https://www.who.int/publications/i/item/9789240060241. Retrieved 19
757 September 2025.

758 8. Patterson TF, Thompson GR, Denning DW, Fishman JA, Hadley S, Herbrecht R,
759 Kontoyiannis DP, Marr KA, Morrison VA, Nguyen MH, Segal BH, Steinbach WJ, Stevens
760 DA, Walsh TJ, Wingard JR, Young J-AH, Bennett JE. 2016. Practice Guidelines for the
761 Diagnosis and Management of Aspergillosis: 2016 Update by the Infectious Diseases
762 Society of America. Clin Infect Dis 63:e1–e60.

763 9. mcdermott A Drug resistant fungi on the rise - Google Search.
764 https://www.pnas.org/doi/10.1073/pnas.2217948119. Retrieved 19 September 2025.

765 10. Lee Y, Robbins N, Cowen LE. 2023. Molecular mechanisms governing antifungal drug
766 resistance. npj Antimicrob Resist 1:5.

767 11. Warrilow AGS, Parker JE, Price CL, Nes WD, Kelly SL, Kelly DE. 2015. In Vitro
768 Biochemical Study of CYP51-Mediated Azole Resistance in Aspergillus fumigatus.
769 Antimicrobial Agents and Chemotherapy 59:7771–7778.

770 12. Verweij PE, Lucas JA, Arendrup MC, Bowyer P, Brinkmann AJF, Denning DW, Dyer PS,
771 Fisher MC, Geenen PL, Gisi U, Hermann D, Hoogendijk A, Kiers E, Lagrou K, Melchers
772 WJG, Rhodes J, Rietveld AG, Schoustra SE, Stenzel K, Zwaan BJ, Fraaije BA. 2020. The
773 one health problem of azole resistance in Aspergillus fumigatus: current insights and
774 future research agenda. Fungal Biology Reviews 34:202–214.

775 13. Mellado E, Garcia-Effron G, Alcázar-Fuoli L, Melchers WJG, Verweij PE, Cuenca-Estrella
776 M, Rodríguez-Tudela JL. 2007. A new Aspergillus fumigatus resistance mechanism
777 conferring in vitro cross-resistance to azole antifungals involves a combination of
778 cyp51A alterations. Antimicrob Agents Chemother 51:1897–1904.

779 14. Chowdhary A, Sharma C, Meis JF. 2017. Azole-Resistant Aspergillosis: Epidemiology,
780 Molecular Mechanisms, and Treatment. J Infect Dis 216:S436–S444.

781 15. Gsaller F, Hortschansky P, Furukawa T, Carr PD, Rash B, Capilla J, Müller C, Bracher F,
782 Bowyer P, Haas H, Brakhage AA, Bromley MJ. 2016. Sterol Biosynthesis and Azole
783 Tolerance Is Governed by the Opposing Actions of SrbA and the CCAAT Binding
784 Complex. PLOS Pathogens 12:e1005775.

785 16. Blosser SJ, Cramer RA. 2012. SREBP-Dependent Triazole Susceptibility in Aspergillus
786 fumigatus Is Mediated through Direct Transcriptional Regulation of erg11A (cyp51A).
787 Antimicrob Agents Chemother 56:248–257.

788 17. Blatzer M, Barker BM, Willger SD, Beckmann N, Blosser SJ, Cornish EJ, Mazurie A, Grahl
789 N, Haas H, Cramer RA. 2011. SREBP coordinates iron and ergosterol homeostasis to

790 mediate triazole drug and hypoxia responses in the human fungal pathogen
791 Aspergillus fumigatus. PLoS Genet 7:e1002374.

792 18. Paul S, Stamnes M, Thomas GH, Liu H, Hagiwara D, Gomi K, Filler SG, Moye-Rowley
793 WS. 2019. AtrR Is an Essential Determinant of Azole Resistance in Aspergillus
794 fumigatus. mBio 10:10.1128/mbio.02563-18.

795 19. Birštonas L, Hortschansky P, Bauer I, Alcanzo EM, Kühbacher A, Mertens B, Müller C,
796 Brakhage AA, Gsaller F. 2025. The transcription factor RttA contributes to sterol
797 regulation and azole resistance in Aspergillus fumigatus. mBio.

798 20. Willger SD, Puttikamonkul S, Kim K-H, Burritt JB, Grahl N, Metzler LJ, Barbuch R, Bard M,
799 Lawrence CB, Jr RAC. 2008. A Sterol-Regulatory Element Binding Protein Is Required
800 for Cell Polarity, Hypoxia Adaptation, Azole Drug Resistance, and Virulence in
801 Aspergillus fumigatus. PLOS Pathogens 4:e1000200.

802 21. Yan R, Cao P, Song W, Li Y, Wang T, Qian H, Yan C, Yan N. 2021. Structural basis for
803 sterol sensing by Scap and Insig. Cell Rep 35:109299.

804 22. Butler G. 2013. Hypoxia and Gene Expression in Eukaryotic Microbes. Annu Rev
805 Microbiol 67:291–312.

806 23. Sever N, Yang T, Brown MS, Goldstein JL, DeBose-Boyd RA. 2003. Accelerated
807 degradation of HMG CoA reductase mediated by binding of insig-1 to its sterol-sensing
808 domain. Mol Cell 11:25–33.

809 24. Rybak JM, Ge W, Wiederhold NP, Parker JE, Kelly SL, Rogers PD, Fortwendel JR. 2019.
810 Mutations in hmg1, Challenging the Paradigm of Clinical Triazole Resistance in
811 Aspergillus fumigatus. mBio 10:10.1128/mbio.00437-19.

812 25. Hagiwara D, Arai T, Takahashi H, Kusuya Y, Watanabe A, Kamei K. 2018. Non-cyp51A
813 Azole-Resistant Aspergillus fumigatus Isolates with Mutation in HMG-CoA Reductase.
814 Emerg Infect Dis 24:1889–1897.

815 26. Gonzalez-Jimenez I, Lucio J, Roldan A, Alcazar-Fuoli L, Mellado E. 2021. Are Point
816 Mutations in HMG-CoA Reductases (Hmg1 and Hmg2) a Step towards Azole
817 Resistance in Aspergillus fumigatus? Molecules 26:5975.

818 27. Souza ACO, Ge W, Wiederhold NP, Rybak JM, Fortwendel JR, Rogers PD. 2023. hapE and
819 hmg1 Mutations Are Drivers of cyp51A-Independent Pan-Triazole Resistance in an
820 Aspergillus fumigatus Clinical Isolate. Microbiology Spectrum 11:e05188-22.

821 28. Rybak JM, Xie J, Martin-Vicente A, Guruceaga X, Thorn HI, Nywening AV, Ge W, Souza
822 ACO, Shetty AC, McCracken C, Bruno VM, Parker JE, Kelly SL, Snell HM, Cuomo CA,
823 Rogers PD, Fortwendel JR. 2024. A secondary mechanism of action for triazole
824 antifungals in Aspergillus fumigatus mediated by hmg1. Nat Commun 15:3642.

825 29. Berman J, Krysan DJ. 2020. Drug resistance and tolerance in fungi. Nat Rev Microbiol
826 18:319–331.

827 30. Scott J, Valero C, Mato-López Á, Donaldson IJ, Roldán A, Chown H, Rhijn NV, Lobo-Vega
828 R, Gago S, Furukawa T, Morogovsky A, Ami RB, Bowyer P, Osherov N, Fontaine T,

829 Goldman GH, Mellado E, Bromley M, Amich J. 2022. Aspergillus fumigatus can display
830 persistence to the fungicidal drug voriconazole. bioRxiv
831 https://doi.org/10.1101/2022.05.16.491816.

832 31. Scott J, Valero C, Mato-López Á, Donaldson IJ, Roldán A, Chown H, Rhijn NV, Lobo-Vega
833 R, Gago S, Furukawa T, Morogovsky A, Ami RB, Bowyer P, Osherov N, Fontaine T,
834 Goldman GH, Mellado E, Bromley M, Amich J. 2023. Aspergillus fumigatus Can
835 Display Persistence to the Fungicidal Drug Voriconazole. Microbiology Spectrum
836 https://doi.org/10.1128/spectrum.04770-22.

837 32. Jöchl C, Rederstorff M, Hertel J, Stadler PF, Hofacker IL, Schrettl M, Haas H,
838 Hüttenhofer A. 2008. Small ncRNA transcriptome analysis from Aspergillus fumigatus
839 suggests a novel mechanism for regulation of protein synthesis. Nucleic Acids Res
840 36:2677–2689.

841 33. Losada L, Barker BM, Pakala S, Pakala S, Joardar V, Zafar N, Mounaud S, Fedorova N,
842 Nierman WC, Cramer RA. 2014. Large-scale transcriptional response to hypoxia in
843 Aspergillus fumigatus observed using RNAseq identifies a novel hypoxia regulated
844 ncRNA. Mycopathologia 178:331–339.

845 34. Basenko EY, Shanmugasundram A, Böhme U, Starns D, Wilkinson PA, Davison HR,
846 Crouch K, Maslen G, Harb OS, Amos B, McDowell MA, Kissinger JC, Roos DS, Jones A.
847 2024. What is new in FungiDB: a web-based bioinformatics platform for omics-scale
848 data analysis for fungal and oomycete species. Genetics 227:iyae035.

849 35. Scotto–Lavino E, Du G, Frohman MA. 2006. 3' End cDNA amplification using classic
850 RACE. Nat Protoc 1:2742–2745.

851 36. Punt PJ, Dingemanse MA, Kuyvenhoven A, Soede RDM, Pouwels PH, van den Hondel
852 CAMJJ. 1990. Functional elements in the promoter region of the *Aspergillus nidulans*
853 *gpdA* gene encoding glyceraldehyde-3-phosphate dehydrogenase. Gene 93:101–109.

854 37. Snarr BD, Baker P, Bamford NC, Sato Y, Liu H, Lehoux M, Gravelat FN, Ostapska H,
855 Baistrocchi SR, Cerone RP, Filler EE, Parsek MR, Filler SG, Howell PL, Sheppard DC.
856 2017. Microbial glycoside hydrolases as antibiofilm agents with cross-kingdom
857 activity. Proc Natl Acad Sci U S A 114:7124–7129.

858 38. Morelli KA, Kerkaert JD, Cramer RA. 2021. Aspergillus fumigatus biofilms: Toward
859 understanding how growth as a multicellular network increases antifungal resistance
860 and disease progression. PLoS Pathog 17:e1009794.

861 39. Langner S, Staber PB, Neumeister P. 2008. Posaconazole in the management of
862 refractory invasive fungal infections. Ther Clin Risk Manag 4:747–758.

863 40. Xiao L, Madison V, Chau AS, Loebenberg D, Palermo RE, McNicholas PM. 2004. Three-
864 Dimensional Models of Wild-Type and Mutated Forms of Cytochrome P450 14α-Sterol
865 Demethylases from Aspergillus fumigatus and Candida albicans Provide Insights into
866 Posaconazole Binding. Antimicrob Agents Chemother 48:568–574.

867 41. Dhingra S, Kowalski CH, Thammahong A, Beattie SR, Bultman KM, Cramer RA. 2016.
868 RbdB, a Rhomboid Protease Critical for SREBP Activation and Virulence in Aspergillus
869 fumigatus. mSphere 1:e00035-16.

870 42. Dhingra S, Buckey JC, Cramer RA. 2018. Hyperbaric Oxygen Reduces Aspergillus
871 fumigatus Proliferation In Vitro and Influences In Vivo Disease Outcomes. Antimicrob
872 Agents Chemother 62:e01953-17.

873 43. Graybill JR, Najvar LK, Gonzalez GM, Hernandez S, Bocanegra R. 2003. Improving the
874 mouse model for studying the efficacy of voriconazole. J Antimicrob Chemother
875 51:1373–1376.

876 44. Bertuzzi M, van Rhijn N, Krappmann S, Bowyer P, Bromley MJ, Bignell EM. 2020. On the
877 lineage of Aspergillus fumigatus isolates in common laboratory use. Med Mycol 59:7–
878 13.

879 45. Keller NP. 2017. Heterogeneity Confounds Establishment of "a" Model Microbial Strain.
880 mBio 8:10.1128/mbio.00135-17.

881 46. Manente M, Ghislain M. 2009. The lipid-translocating exporter family and membrane
882 phospholipid homeostasis in yeast. FEMS Yeast Res 9:673–687.

883 47. Hokken MWJ, Zoll J, Coolen JPM, Zwaan BJ, Verweij PE, Melchers WJG. 2019.
884 Phenotypic plasticity and the evolution of azole resistance in Aspergillus fumigatus;
885 an expression profile of clinical isolates upon exposure to itraconazole. BMC
886 Genomics 20:28.

887 48. Ness F, Aigle M. 1995. Rtm1: A Member of a New Family of Telomeric Repeated Genes
888 in Yeast. Genetics 140:945–956.

889 49. Abou-Kandil A, Tröger-Görler S, Pschibul A, Krüger T, Rosin M, Schmidt F,
890 Akbarimoghaddam P, Sarkar A, Cseresnyés Z, Shadkchan Y, Heinekamp T, Gräler MH,
891 Barber AE, Walther G, Figge MT, Brakhage AA, Osherov N, Kniemeyer O. 2025. The
892 proteomic response of Aspergillus fumigatus to amphotericin B (AmB) reveals the
893 involvement of the RTA-like protein RtaA in AmB resistance. microLife 6:uqae024.

894 50. Bueid A, Howard SJ, Moore CB, Richardson MD, Harrison E, Bowyer P, Denning DW.
895 2010. Azole antifungal resistance in Aspergillus fumigatus: 2008 and 2009. J
896 Antimicrob Chemother 65:2116–2118.

897 51. Burks C, Darby A, Londoño LG, Momany M, Brewer MT. 2021. Azole-resistant
898 Aspergillus fumigatus in the environment: Identifying key reservoirs and hotspots of
899 antifungal resistance. PLOS Pathogens 17:e1009711.

900 52. Brauner A, Fridman O, Gefen O, Balaban NQ. 2016. Distinguishing between resistance,
901 tolerance and persistence to antibiotic treatment. Nat Rev Microbiol 14:320–330.

902 53. Geißel B, Loiko V, Klugherz I, Zhu Z, Wagener N, Kurzai O, van den Hondel CAMJJ,
903 Wagener J. 2018. Azole-induced cell wall carbohydrate patches kill Aspergillus
904 fumigatus. Nat Commun 9:3098.

905 54. Umeyama T, Hayashi Y, Shimosaka H, Inukai T, Yamagoe S, Takatsuka S, Hoshino Y,
906 Nagi M, Nakamura S, Kamei K, Ogawa K, Miyazaki Y. 2018. CRISPR/Cas9 Genome

907 Editing To Demonstrate the Contribution of Cyp51A Gly138Ser to Azole Resistance in
908 Aspergillus fumigatus. Antimicrobial Agents and Chemotherapy
909 https://doi.org/10.1128/aac.00894-18.

910 55. Mowat E, Butcher J, Lang S, Williams C, Ramage G. 2007. Development of a simple
911 model for studying the effects of antifungal agents on multicellular communities of
912 Aspergillus fumigatus. Journal of Medical Microbiology 56:1205–1212.

913 56. Liu S, Le Mauff F, Sheppard DC, Zhang S. 2022. Filamentous fungal biofilms: Conserved
914 and unique aspects of extracellular matrix composition, mechanisms of drug
915 resistance and regulatory networks in Aspergillus fumigatus. npj Biofilms
916 Microbiomes 8:83.

917 57. Wuyts J, Van Dijck P, Holtappels M. 2018. Fungal persister cells: The basis for
918 recalcitrant infections? PLoS Pathog 14:e1007301.

919 58. De Francesco MA. 2023. Drug-Resistant Aspergillus spp.: A Literature Review of Its
920 Resistance Mechanisms and Its Prevalence in Europe. Pathogens 12:1305.

921 59. Dagenais TRT, Keller NP. 2009. Pathogenesis of Aspergillus fumigatus in Invasive
922 Aspergillosis. Clin Microbiol Rev 22:447–465.

923 60. Kowalski CH, Beattie SR, Fuller KK, McGurk EA, Tang Y-W, Hohl TM, Obar JJ, Cramer RA.
924 2016. Heterogeneity among Isolates Reveals that Fitness in Low Oxygen Correlates
925 with Aspergillus fumigatus Virulence. mBio 7:10.1128/mbio.01515-16.

926 61. Caffrey-Carr AK, Kowalski CH, Beattie SR, Blaseg NA, Upshaw CR, Thammahong A,
927 Lust HE, Tang Y-W, Hohl TM, Cramer RA, Obar JJ. 2017. Interleukin 1α Is Critical for
928 Resistance against Highly Virulent Aspergillus fumigatus Isolates. Infect Immun
929 85:e00661-17.

930 62. Fuller KK, Cramer RA, Zegans ME, Dunlap JC, Loros JJ. 2016. Aspergillus fumigatus
931 Photobiology Illuminates the Marked Heterogeneity between Isolates. mBio 7:e01517-
932 16.

933 63. Traubenik S, Charon C, Blein T. 2024. From environmental responses to adaptation: the
934 roles of plant lncRNAs. Plant Physiol 195:232–244.

935 64. Bowyer P, Weaver D, Qi T, Chown H, Fraczek M, Lebedinec R, Dineen L, Valero C, Rhijn
936 N van, Furukawa T, Bromley M, Delneri D. 2025. Genome-wide discovery and
937 phenotyping of non-coding transcripts in A. fumigatus reveals lncRNAs with a role in
938 antifungal drug sensitivity. Research Square https://doi.org/10.21203/rs.3.rs-
939 6048166/v1.

940 65. Smith-Peavler ES, Patel R, Onumajuru AM, Bowring BG, Miller JL, Brunel JM, Djordjevic
941 JT, Prabu MM, McClelland EE. 2022. RTA1 Is Involved in Resistance to 7-
942 Aminocholesterol and Secretion of Fungal Proteins in Cryptococcus neoformans.
943 Pathogens 11:1239.

944 66. Barber AE, Sae-Ong T, Kang K, Seelbinder B, Li J, Walther G, Panagiotou G, Kurzai O.
945 2021. Aspergillus fumigatus pan-genome analysis identifies genetic variants
946 associated with human infection. Nat Microbiol 6:1526–1536.

947 67. Kowalski CH, Morelli KA, Stajich JE, Nadell CD, Cramer RA. A Heterogeneously
948 Expressed Gene Family Modulates the Biofilm Architecture and Hypoxic Growth of
949 Aspergillus fumigatus. mBio 12:e03579-20.

950 68. Mercer TR, Dinger ME, Mattick JS. 2009. Long non-coding RNAs: insights into functions.
951 Nat Rev Genet 10:155–159.

952 69. Thammahong A, Caffrey-Card AK, Dhingra S, Obar JJ, Cramer RA. 2017. Aspergillus
953 fumigatus Trehalose-Regulatory Subunit Homolog Moonlights To Mediate Cell Wall
954 Homeostasis through Modulation of Chitin Synthase Activity. mBio 8:e00056-17.

955 70. Szewczyk E, Nayak T, Oakley CE, Edgerton H, Xiong Y, Taheri-Talesh N, Osmani SA,
956 Oakley BR. 2006. Fusion PCR and gene targeting in Aspergillus nidulans. Nat Protoc
957 1:3111–3120.

958 71. Thammahong A, Dhingra S, Bultman KM, Kerkaert JD, Cramer RA. 2019. An Ssd1
959 Homolog Impacts Trehalose and Chitin Biosynthesis and Contributes to Virulence in
960 Aspergillus fumigatus. mSphere 4:e00244-19.

961 72. Al Abdallah Q, Ge W, Fortwendel JR. 2017. A Simple and Universal System for Gene
962 Manipulation in Aspergillus fumigatus: In Vitro-Assembled Cas9-Guide RNA

963 Ribonucleoproteins Coupled with Microhomology Repair Templates. mSphere
964 2:e00446-17.

965 73. Furukawa T, van Rhijn N, Chown H, Rhodes J, Alfuraji N, Fortune-Grant R, Bignell E,
966 Fisher MC, Bromley M. 2022. Exploring a novel genomic safe-haven site in the human
967 pathogenic mould Aspergillus fumigatus. Fungal Genet Biol 161:103702.

968 74. Oakley BR, Rinehart JE, Mitchell BL, Oakley CE, Carmona C, Gray GL, May GS. 1987.
969 Cloning, mapping and molecular analysis of the pyrG (orotidine-5'-phosphate
970 decarboxylase) gene of Aspergillus nidulans. Gene 61:385–399.

971 75. Dhingra S, Lind AL, Lin H-C, Tang Y, Rokas A, Calvo AM. 2013. The fumagillin gene
972 cluster, an example of hundreds of genes under veA control in Aspergillus fumigatus.
973 PLoS One 8:e77147.

974 76. Osmani AH, May GS, Osmani SA. 1999. The extremely conserved pyroA gene of
975 Aspergillus nidulans is required for pyridoxine synthesis and is required indirectly for
976 resistance to photosensitizers. J Biol Chem 274:23565–23569.

977 77. Zepeda B, Verdonk JC. 2022. RNA Extraction from Plant Tissue with Homemade Acid
978 Guanidinium Thiocyanate Phenol Chloroform (AGPC). Current Protocols 2:e351.

979 78. STAR: ultrafast universal RNA-seq aligner | Bioinformatics | Oxford Academic.
980 https://academic.oup.com/bioinformatics/article/29/1/15/272537. Retrieved 9
981 September 2025.

79. Danecek P, Bonfield JK, Liddle J, Marshall J, Ohan V, Pollard MO, Whitwham A, Keane T, McCarthy SA, Davies RM, Li H. 2021. Twelve years of SAMtools and BCFtools. Gigascience 10:giab008.

80. Liao Y, Smyth GK, Shi W. 2014. featureCounts: an efficient general purpose program for assigning sequence reads to genomic features. Bioinformatics 30:923–930.

81. Love MI, Huber W, Anders S. 2014. Moderated estimation of fold change and dispersion for RNA-seq data with DESeq2. Genome Biol 15:550.

82. Blighe K, Rana S, Lewis M. EnhancedVolcano: Publication-ready volcano plots with enhanced colouring and labeling https://doi.org/10.18129/B9.bioc.EnhancedVolcano.

83. R Core Team (2024). R: A Language and Environment for Statistical Computing (version 3.5.1). R Foundation for Statistical Computing. https://www.R-project.org/. Retrieved 9 September 2025.

84. Stajich J. 2025. stajichlab/DhingraLab_ncRNA_Afumigatus: Archive of Analysis and Data archive for publication (v0.1). Zenodo.

Acknowledgements:

We would like to acknowledge members of Dhingra laboratory and Eukaryotic Pathogen innovation center for discussions surrounding the experiments in the manuscript. The research in Dhingra lab is supported by start-up funds from the Department of Biological Science at Clemson University and National Institute of General Medical Sciences (NIGMS) award (P20GM146584) (James Morris, Principal Investigator). We thank Dr. Robert Cramer at the Dartmouth Geisel School of Medicine (NIAID/NIH grants R01AI181215 and 2R0AI130128) for providing resources and critical reading of the manuscript. The Clemson University Genomics and Bioinformatics Facility is supported by the College of Science and Grants P20GM146584 and P20GM139769 Institutional Development Awards (IDeA) from the National Institute of General Medical Sciences of the National Institutes of Health. This work was supported, in part, by equipment housed in the Clemson Light Imaging Facility. We utilized a Leica Laser Microdissection system for brightfield imaging, and a Leica Pearl Automatic Tissue Processor and a Leica Histocore Biocut Rotary Microtome for histology preparation. Thank you to Mr. Avery Herren for assistance with histology. The Clemson Light Imaging Facility is supported by the Division of Research and EPIC COBRE P20GM146584. We thank Dr. Jarrod Fortwendel for the Fdel262 strain, and Dr. James Morris for the critical reading of the manuscript. The funding sources had no role in the study design, data collection and interpretation, preparation of this manuscript or the decision to submit the manuscript.

Figure 1:

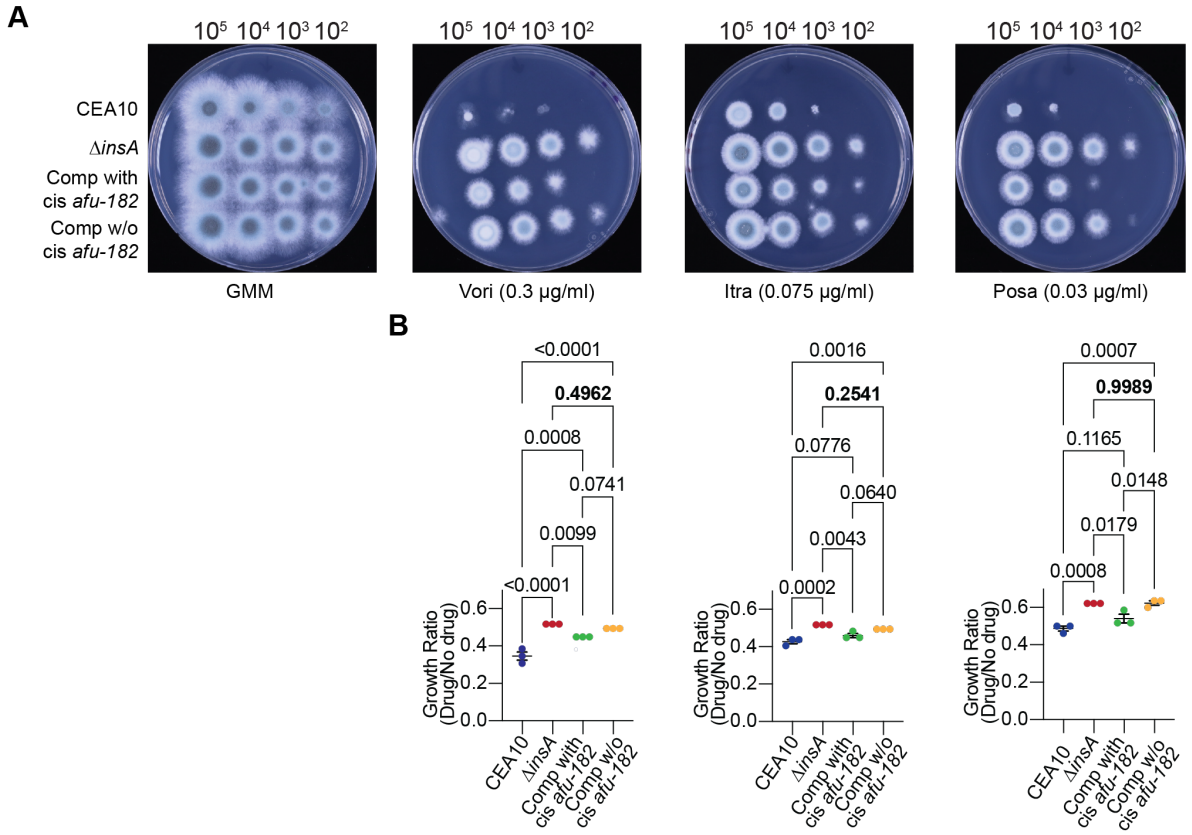
A
10^5 10^4 10^3 10^2
CEA10
ΔinsA
Comp with cis afu-182
Comp w/o cis afu-182
GMM
Vori (0.3 μg/ml)
Itra (0.075 μg/ml)
Posa (0.03 μg/ml)
B
Growth Ratio (Drug/No drug)
0.0
0.2
0.4
0.6
<0.0001
0.4962
0.0008
0.0741
0.0099
<0.0001
0.0016
0.2541
0.0776
0.0640
0.0043
0.0002
0.0007
0.9989
0.1165
0.0148
0.0179
0.0008
CEA10
ΔinsA
Comp with cis afu-182
Comp w/o cis afu-182

Figure 2:

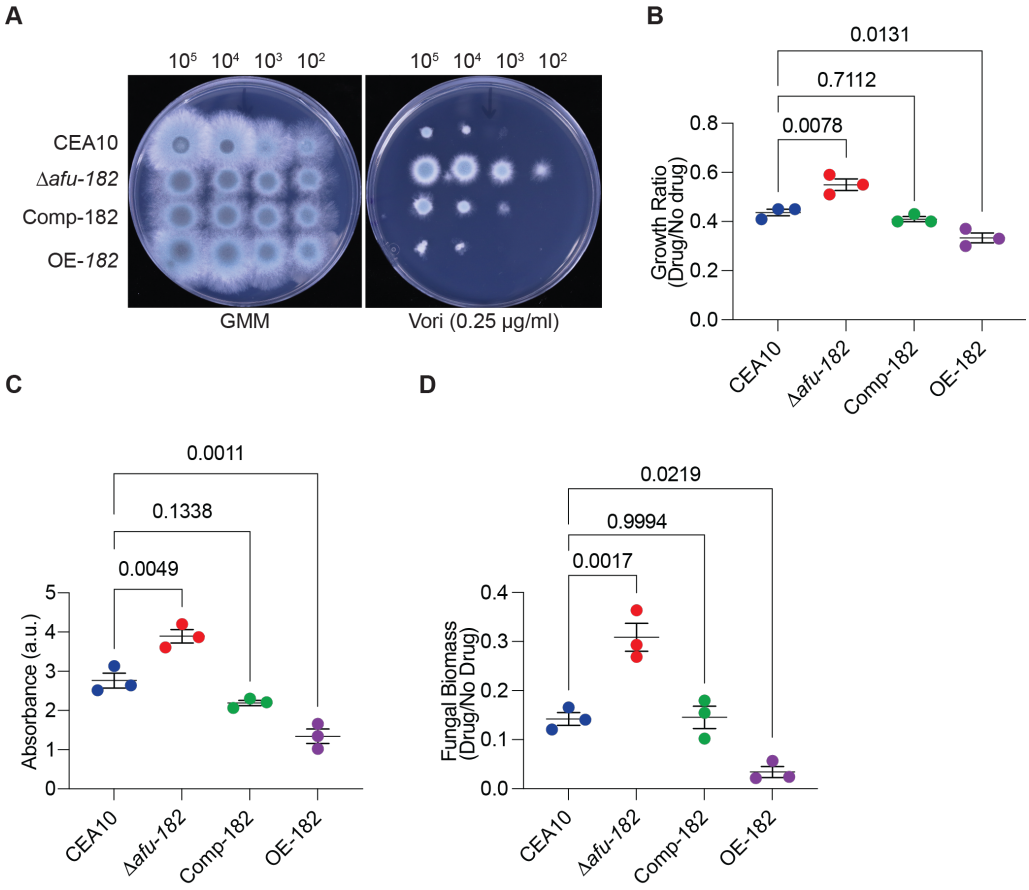
A
10⁵ 10⁴ 10³ 10²
10⁵ 10⁴ 10³ 10²
CEA10
Δafu-182
Comp-182
OE-182
GMM
Vori (0.25 µg/ml)
B
0.0131
0.7112
0.0078
Growth Ratio (Drug/No drug)
0.8
0.6
0.4
0.2
0.0
CEA10
Δafu-182
Comp-182
OE-182
C
0.0011
0.1338
0.0049
Absorbance (a.u.)
5
4
3
2
1
0
CEA10
Δafu-182
Comp-182
OE-182
D
0.0219
0.9994
0.0017
Fungal Biomass (Drug/No Drug)
0.4
0.3
0.2
0.1
0.0
CEA10
Δafu-182
Comp-182
OE-182

Figure 3:

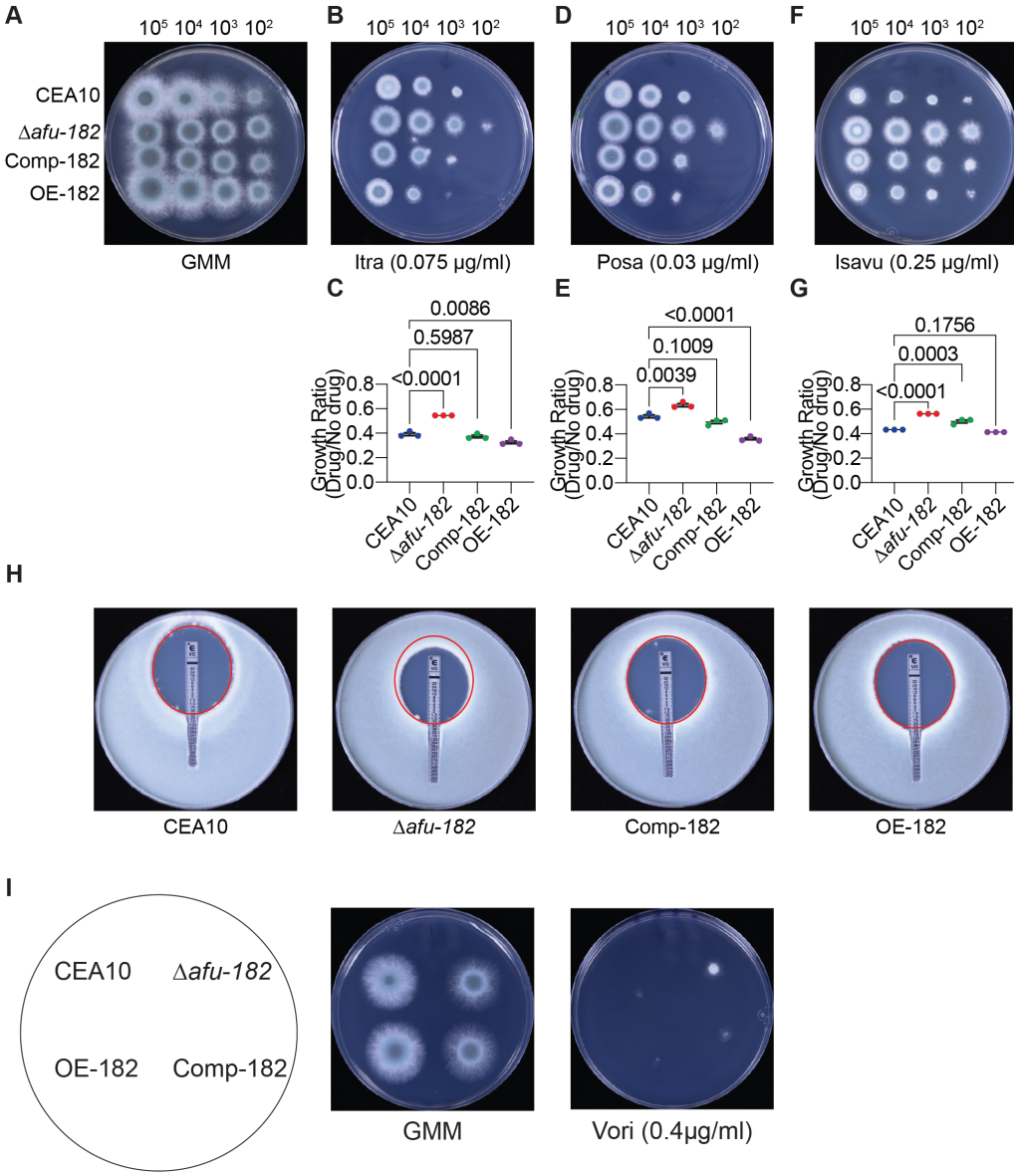
A
B
D
F
10^5 10^4 10^3 10^2
CEA10
Δafu-182
Comp-182
OE-182
GMM
Itra (0.075 µg/ml)
Posa (0.03 µg/ml)
Isavu (0.25 µg/ml)
C
E
G
Growth Ratio (Drug/No drug)
0.0
0.2
0.4
0.6
0.8
0.0086
0.5987
<0.0001
<0.0001
0.1009
0.0039
0.1756
0.0003
<0.0001
CEA10
Δafu-182
Comp-182
OE-182
H
CEA10
Δafu-182
Comp-182
OE-182
I
CEA10
Δafu-182
OE-182
Comp-182
GMM
Vori (0.4µg/ml)

Figure 4:

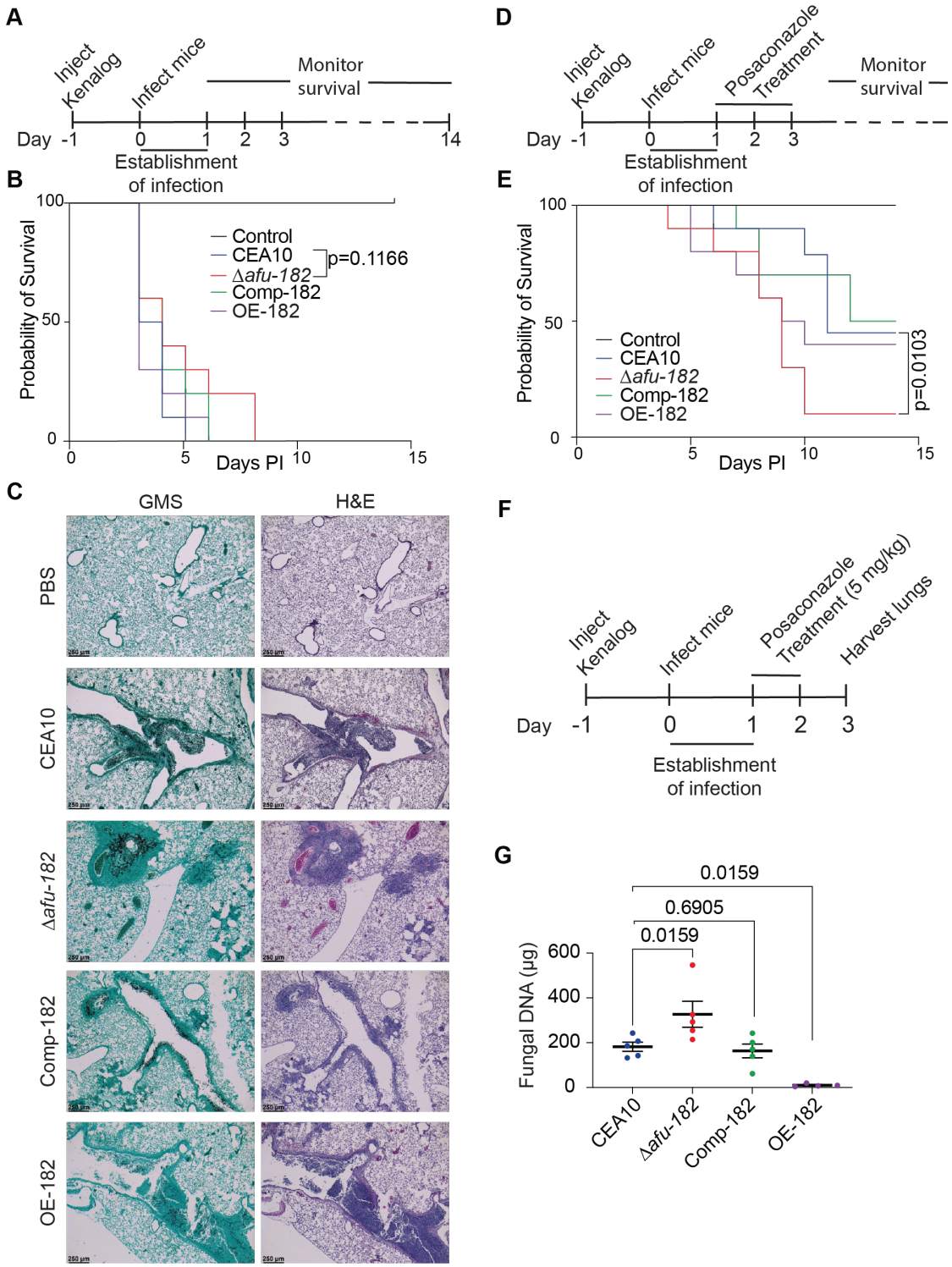
A
Inject Kenalog
Infect mice
Monitor survival
Day -1 0 1 2 3 14
Establishment of infection
B
Probability of Survival
Control
CEA10
Δafu-182
Comp-182
OE-182
p=0.1166
Days PI
C
GMS
H&E
PBS
CEA10
Δafu-182
Comp-182
OE-182
D
Inject Kenalog
Infect mice
Posaconazole Treatment
Monitor survival
Day -1 0 1 2 3
Establishment of infection
E
Probability of Survival
Control
CEA10
Δafu-182
Comp-182
OE-182
p=0.0103
Days PI
F
Inject Kenalog
Infect mice
Posaconazole Treatment (5 mg/kg)
Harvest lungs
Day -1 0 1 2 3
Establishment of infection
G
Fungal DNA (µg)
0.0159
0.6905
0.0159
CEA10
Δafu-182
Comp-182
OE-182

Figure 5:

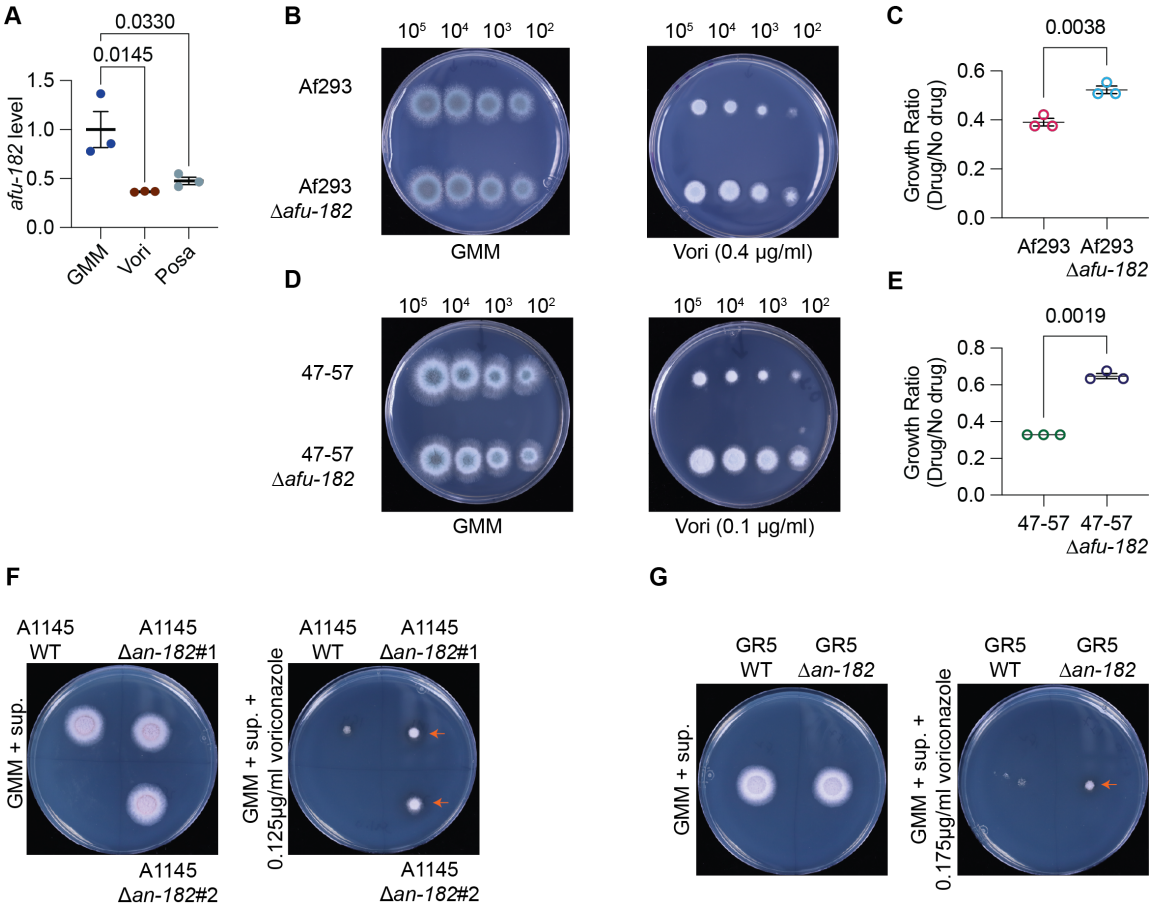
A
0.0330
0.0145
1.5
1.0
0.5
0.0
afu-182 level
GMM
Vori
Posa
B
10⁵ 10⁴ 10³ 10²
Af293
Af293
Δafu-182
GMM
Vori (0.4 µg/ml)
C
0.0038
Growth Ratio
(Drug/No drug)
0.6
0.4
0.2
0.0
Af293
Af293
Δafu-182
D
10⁵ 10⁴ 10³ 10²
47-57
47-57
Δafu-182
GMM
Vori (0.1 µg/ml)
E
0.0019
Growth Ratio
(Drug/No drug)
0.8
0.6
0.4
0.2
0.0
47-57
47-57
Δafu-182
F
A1145
WT
A1145
Δan-182#1
GMM + sup.
A1145
Δan-182#2
GMM + sup. +
0.125µg/ml voriconazole
G
GR5
WT
GR5
Δan-182
GMM + sup.
GMM + sup. +
0.175µg/ml voriconazole

Figure 6:

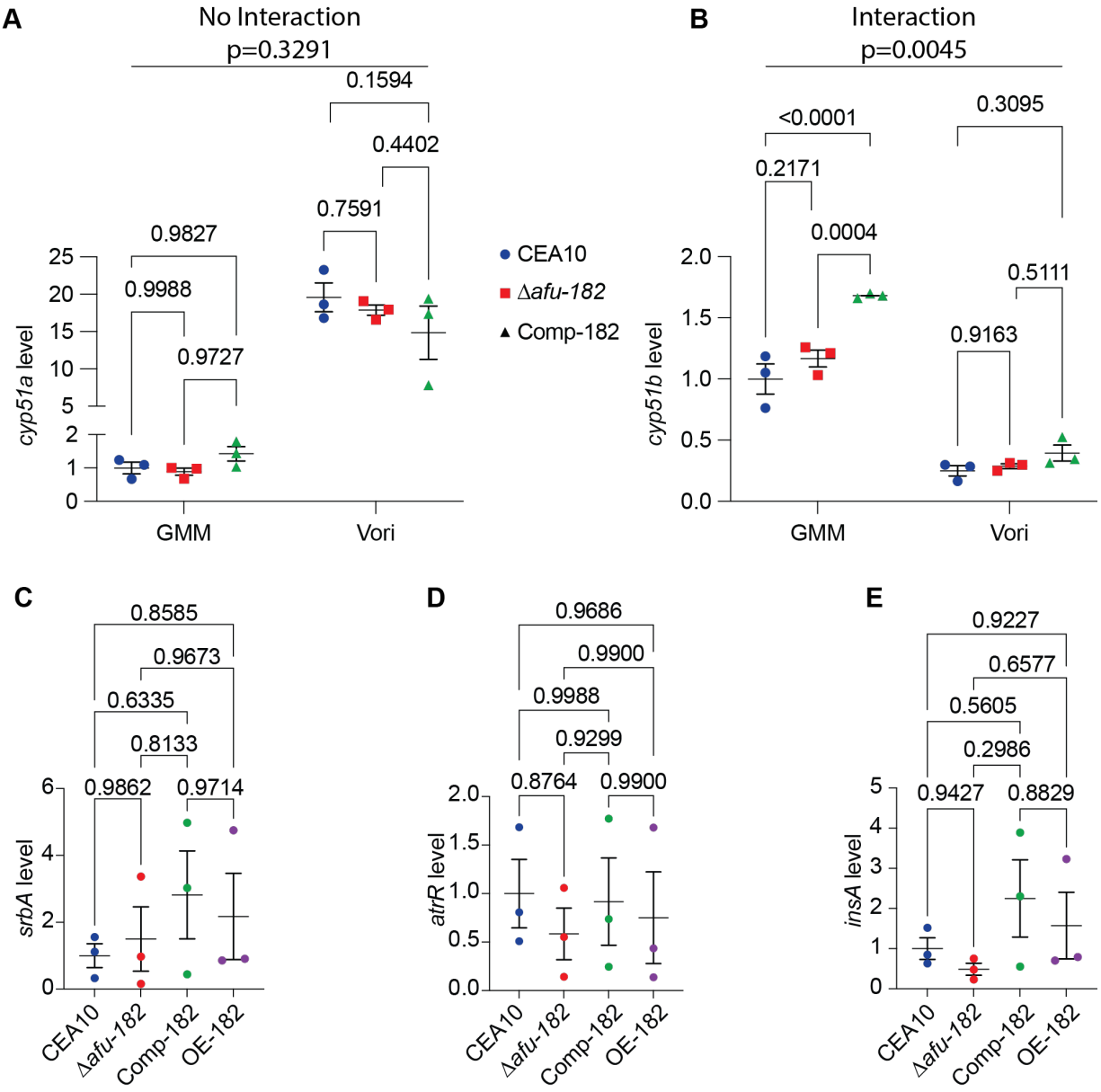
A
No Interaction
p=0.3291
0.1594
0.4402
0.7591
0.9827
0.9988
0.9727
cyp51a level
25
20
15
10
5
2
1
0
GMM
Vori
CEA10
Δafu-182
Comp-182
B
Interaction
p=0.0045
<0.0001
0.3095
0.2171
0.0004
0.5111
0.9163
cyp51b level
2.0
1.5
1.0
0.5
0.0
GMM
Vori
C
0.8585
0.9673
0.6335
0.8133
0.9862
0.9714
srbA level
6
4
2
0
CEA10
Δafu-182
Comp-182
OE-182
D
0.9686
0.9900
0.9988
0.9299
0.8764
0.9900
atrR level
2.0
1.5
1.0
0.5
0.0
CEA10
Δafu-182
Comp-182
OE-182
E
0.9227
0.6577
0.5605
0.2986
0.9427
0.8829
insA level
5
4
3
2
1
0
CEA10
Δafu-182
Comp-182
OE-182

Figure 7:

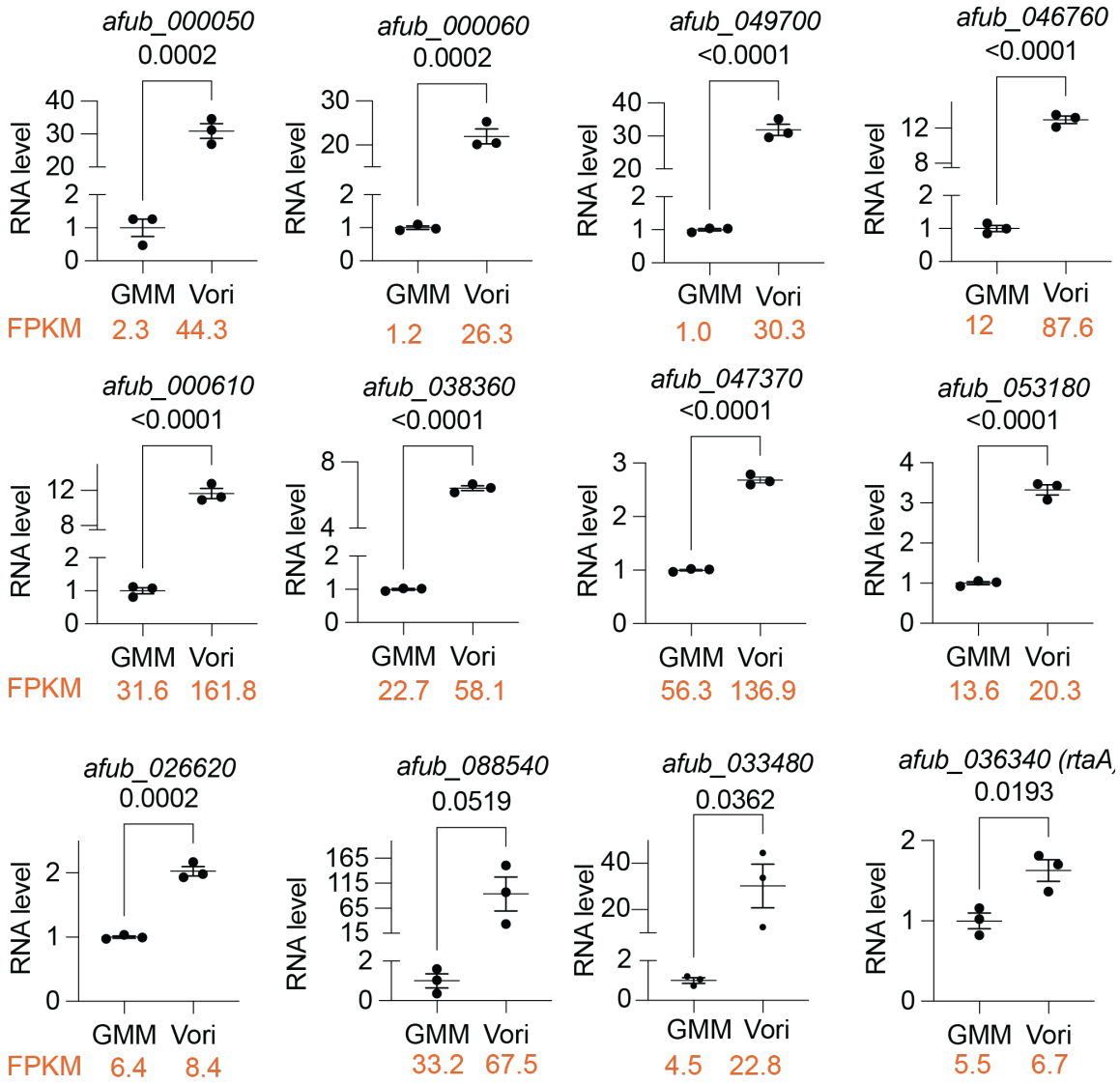
afub_000050
0.0002
RNA level
40
30
20
2
1
0
GMM Vori
FPKM 2.3 44.3
afub_000060
0.0002
RNA level
30
20
2
1
0
GMM Vori
1.2 26.3
afub_049700
<0.0001
RNA level
40
30
20
2
1
0
GMM Vori
1.0 30.3
afub_046760
<0.0001
RNA level
12
8
2
1
0
GMM Vori
12 87.6
afub_000610
<0.0001
RNA level
12
8
2
1
0
GMM Vori
FPKM 31.6 161.8
afub_038360
<0.0001
RNA level
8
4
2
1
0
GMM Vori
22.7 58.1
afub_047370
<0.0001
RNA level
3
2
1
0
GMM Vori
56.3 136.9
afub_053180
<0.0001
RNA level
4
3
2
1
0
GMM Vori
13.6 20.3
afub_026620
0.0002
RNA level
2
1
0
GMM Vori
FPKM 6.4 8.4
afub_088540
0.0519
RNA level
165
115
65
15
2
0
GMM Vori
33.2 67.5
afub_033480
0.0362
RNA level
40
20
2
0
GMM Vori
4.5 22.8
afub_036340 (rtaA
0.0193
RNA level
2
1
0
GMM Vori
5.5 6.7

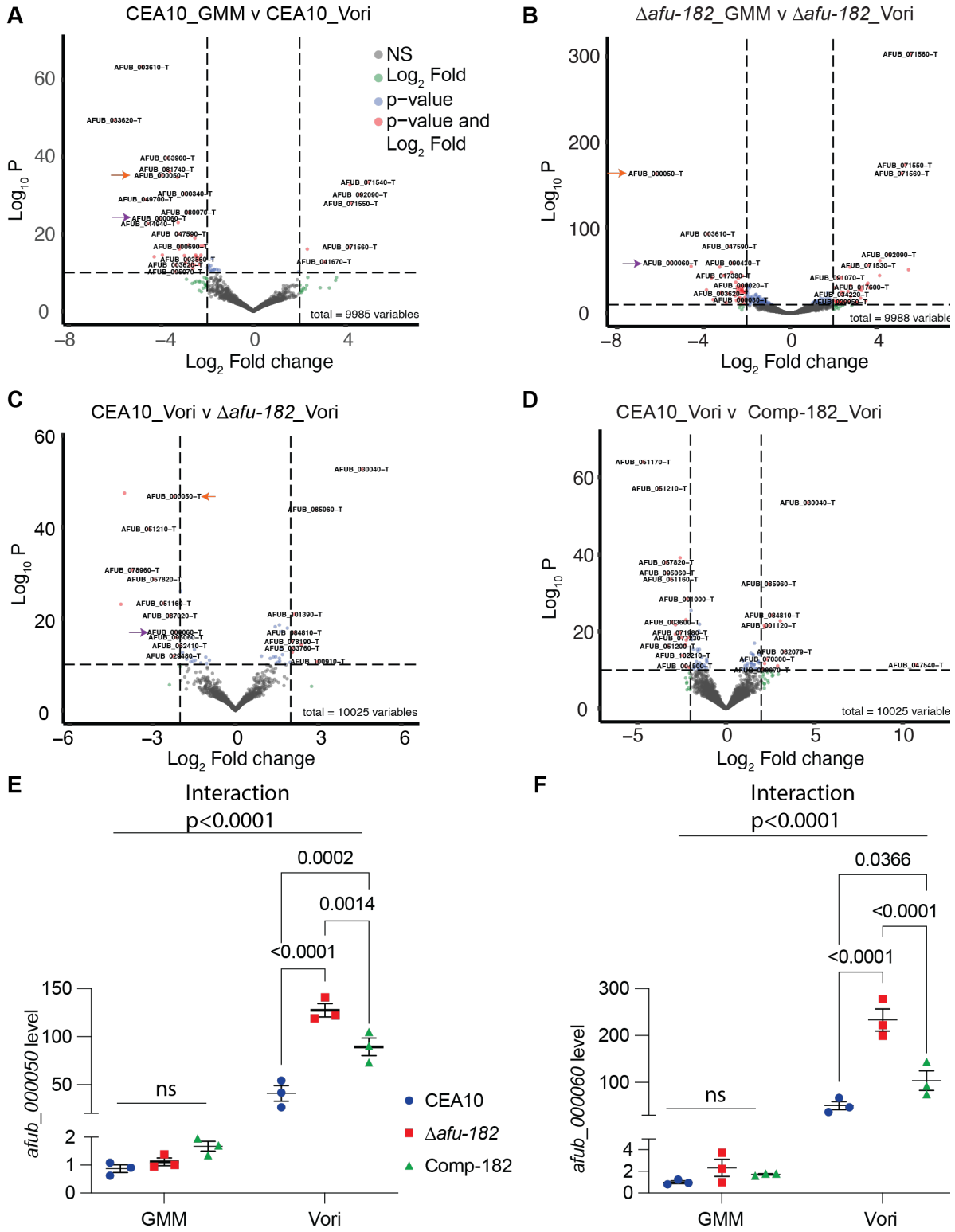
A
CEA10_GMM v CEA10_Vori
NS
Log2 Fold
p−value
p−value and Log2 Fold
Log10 P
Log2 Fold change
total = 9985 variables
B
Δafu-182_GMM v Δafu-182_Vori
Log10 P
Log2 Fold change
total = 9988 variable
C
CEA10_Vori v Δafu-182_Vori
Log10 P
Log2 Fold change
total = 10025 variables
D
CEA10_Vori v Comp-182_Vori
Log10 P
Log2 Fold change
total = 10025 variable
E
Interaction
p<0.0001
0.0002
0.0014
<0.0001
ns
afub_000050 level
GMM
Vori
CEA10
Δafu-182
Comp-182
F
Interaction
p<0.0001
0.0366
<0.0001
<0.0001
ns
afub_000060 level
GMM
Vori

Figure 9:

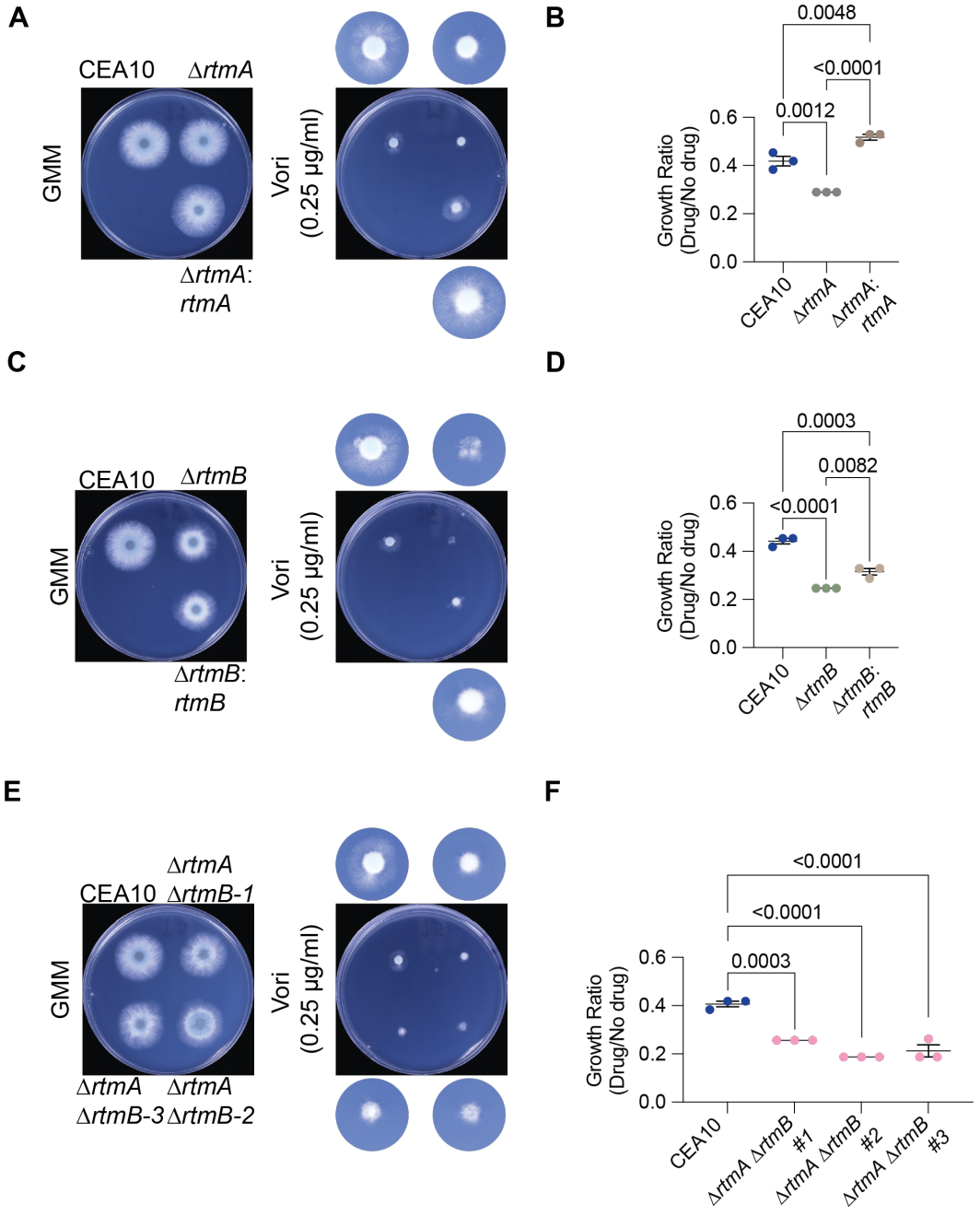
A
CEA10
ΔrtmA
GMM
Vori
(0.25 µg/ml)
ΔrtmA:
rtmA
B
0.0048
<0.0001
0.0012
Growth Ratio
(Drug/No drug)
0.6
0.4
0.2
0.0
CEA10
ΔrtmA
ΔrtmA:
rtmA
C
CEA10
ΔrtmB
GMM
Vori
(0.25 µg/ml)
ΔrtmB:
rtmB
D
0.0003
0.0082
<0.0001
Growth Ratio
(Drug/No drug)
0.6
0.4
0.2
0.0
CEA10
ΔrtmB
ΔrtmB:
rtmB
E
ΔrtmA
CEA10
ΔrtmB-1
GMM
Vori
(0.25 µg/ml)
ΔrtmA
ΔrtmB-3
ΔrtmA
ΔrtmB-2
F
<0.0001
<0.0001
0.0003
Growth Ratio
(Drug/No drug)
0.6
0.4
0.2
0.0
CEA10
ΔrtmA ΔrtmB
#1
ΔrtmA ΔrtmB
#2
ΔrtmA ΔrtmB
#3

Figure Legends:

Figure 1. *afu-182* plays a part in *insA*-mediated fungal azole response. (A) AF strains were serially inoculated (10^5 – 10^2) on GMM in the absence and presence of azole drugs as indicated. As previously reported, the Δ*insA* strain showed increased growth in the presence of azole drugs; however, complementation of *insA* without cis-acting *afu-182* does not revert the phenotype back to WT, whereas complementation of *insA* with cis-acting *afu-182* reverts the phenotype back to WT levels. (B) Graphical representation showing growth ratio calculated by dividing the fungal colony diameter in the presence of the drug by the colony diameter on GMM alone. One-way ANOVA was used to assess the difference in the mean, followed by Tukey's post-hoc analysis to determine pairwise differences. All pairwise comparisons are shown (numbers represent p-values between groups). Bold p-values show no difference between Δ*afu-182* and comp-*insA* without cis-acting *afu-182*.

Figure 2. *afu-182* is sufficient to generate fungal ARC in response to voriconazole. (A) Serially diluted spores (10^5-10^2) were spot inoculated on GMM or GMM + voriconazole (0.25μg/ml, 0.5x MIC) and grown for 48 hours at 37°C. The Δ*afu-182* strain showed increased fungal ARC in the presence of the drug, whereas the OE-182 strain is more inhibited compared to the WT strain. (B) Growth ratio. Colony diameters were measured for colonies as grown in A (for 10^4 spore density) and represented as growth ratio (Drug/no drug). (C) *afu-182* plays a role in fungal biofilm response to azole drugs. AF strains were allowed to adhere to cell culture plates, and biofilms were treated with voriconazole and stained with crystal violet. The OD_{600} values are represented. Δ*afu-182* formed azole recalcitrant biofilms (p=0.0049), whereas OE-182 showed a significant decrease in biofilm formation (p=0.0011) when treated with voriconazole. (D) AF strains were grown in liquid submerged culture with continuous shaking in the presence or absence of 0.2μg/ml voriconazole. After 48 hours, fungal biomass was collected and lyophilized. Dry weight ratio (Drug/no drug) is represented. One-way ANOVA was used to assess the differences in

mean; p-values are listed for all samples compared to WT (One-Way ANOVA followed by Tukey post-hoc analysis). a.u. – arbitrary units.

Figure 3. *afu-182* mediates pan-azole fungal ARC. Serially diluted AF spores (10^5-10^2) of indicated strains were plated on (A) GMM, (B) GMM + itraconazole, (D) GMM + posaconazole, and (F) GMM + isavuconazole. All plates were incubated at 37°C for 48 hours and photographed. Colony diameters were measured and represented as growth ratio between drug and no drug control for (C) itraconazole, (E) posaconazole, and (G) Isavuconazole. One-way ANOVA was used to assess the differences in mean; p-values are listed for all samples compared to WT (Tukey post-hoc analysis). (H) Fungal ARC is not associated with changes in MIC value. GMM plates were inoculated with AF strains as the top agar. Upon agar solidification, E-test strips were laid in the center, and plates were incubated for 48 hours at 37°C. MIC values were determined at the point where the zone of inhibition intersects with the test strip. No MIC above the clinical resistance cutoff was observed; a smaller zone of inhibition (ZOI) was observed in the Δ*afu-182* strain (fungal growth inside the ellipse). (I) Δ*afu-182* can grow at increased drug concentrations. AF strains were inoculated on GMM and GMM + 0.4 μg/ml voriconazole. The drug concentration almost completely inhibited the growth of WT and comp-182 strains; however, the Δ*afu-182* strain showed robust growth.

Figure 4. *afu-182* is dispensable for fungal pathogenesis, but the Δ*afu-182* strain is more virulent upon azole treatment in a corticosteroid murine model of IPA. (A) Schematic showing experimental details for animal infection. (B) Kaplan-Meier plot of animal survival probability for animals infected as in A. No significant difference was observed ($p>0.05$, log-rank test). (C) Histopathological analysis of murine lungs harvested as described in A. No qualitative differences were seen. (D) Schematic showing experimental details for animal infection and azole treatment. (E) Kaplan-Meier plot of animal survival probability for animals infected as in D. A significantly higher mortality (90% vs 55%) was observed in animals infected with the Δ*afu-182* strain compared to animals

infected with the WT strain (p=0.0103, log-rank test). No difference was observed in the mice infected with the OE-182 strain compared to WT (40% mortality vs 50% mortality, p=0.4065). (F) Schematic showing experimental details for infection and treatment. (G) Mice were infected and treated as in F. Fungal DNA was quantified as described in Methods. Significantly more fungal DNA was recovered from animals infected with the Δ*afu-182* strains (p = 0.0159, Mann-Whitney U-test), and significantly less DNA was recovered from animals infected with the OE-182 strain (p = 0.0159, Mann-Whitney U-test) after posaconazole treatment. No difference was observed in fungal DNA isolated from animals infected with WT or comp *afu-182* strains (p=0.6905).

Fig 5. *afu-182* RNA levels are negatively regulated by azoles, and *afu-182* regulates fungal ARC irrespective of the strain's background in multiple Aspergilli. (A) Quantitative reverse transcriptase PCR was used to determine the *afu-182* RNA levels in the WT strain grown in the absence and presence of azoles. Significant downregulation of *afu-182* was observed in the presence of voriconazole (p=0.0145, One-Way ANOVA) and posaconazole (p=0.0330, One-Way ANOVA). *afu-182* was deleted from laboratory reference strain Af293.1 and environmental isolate 47-57. WT and corresponding deletion strains of (B) Af293 and (D) 47-57 were serially inoculated on GMM in the absence and presence of drug, showing fungal ARC irrespective of the strains' background. Growth ratio represented as the ratio of colony diameter in the presence of drug over no drug is represented for (C) Af293 and (E) 47-57. Significantly more growth was observed in Δ*afu-182* strains (two-tailed t-test, p =0.0038 and 0.0019, respectively). *afu-182* homolog (*an-182*) was identified in the related fungal species *Aspergillus nidulans*. *an-182* was deleted in A1145 or GR5 strains of AN. (F and G) 10^4 spores of the indicated strains were spot inoculated on GMM with supplements (see methods) in the absence and presence of voriconazole. Increased fungal ARC was observed in both AN strains (orange arrows).

Figure 6. *afu-182* regulates fungal ARC independent of *cyp51* transcriptional regulation. Quantitative reverse transcriptase was used to determine the mRNA levels of

(A) *cyp51a* and (B) *cyp51b* in the presence or absence of azole drugs. No significant difference due to genotype was observed for *cyp51a* (interaction p=0.3291, Two-Way ANOVA), and an interaction was observed between drug and genotype factors for *cyp51b* (interaction p=0.0045, Two-Way ANOVA). mRNA levels of (C) *srbA*, (D) *atrR*, and (F) *insA* were similarly quantified in GMM. No significant difference was observed between WT and Δ*afu-182* strains (One-Way ANOVA followed by Tukey's post hoc analysis). P-values for pairwise comparison are shown.

Fig 7. Genes encoding RTA1 domain proteins are upregulated in response to voriconazole. Quantitative reverse transcription PCR was used to determine the mRNA levels of RTA1 genes in the presence and absence of azoles. Out of 23, we selected 12 genes that have an FPKM value >1. Eleven of the 12 genes showed significant upregulation in the presence of azoles ($p<0.05$, two-tailed Student's t-test). Importantly, *rtaA,* which plays a role in polyene response but not azole response, showed the lowest upregulation (1.6 fold, p=0.0193, two-tailed student's t-test). Numbers in orange represent the FPKM values from the RNAseq data set.

Figure 8. *afu-182* negatively regulates genes encoding for RTM1 proteins. Volcano plots showing the 2-$\log_2$ fold change (4-fold upregulated or downregulated). (A) Comparison between CEA10 GMM and CEA10 azole. Of the 23 genes encoding RTA1 domain proteins and 11 showing significant change compared to GMM, global analysis revealed genes encoding RTM1 domain proteins *rtmA* (*afub_000050,* orange arrow) and *rtmB* (*afub_000060,* purple arrow) are significantly upregulated. (B) Comparison between Δ*afu-182* GMM and Δ*afu-182* azoles. *rtmA* (orange arrow) and *rtmB* (purple arrow) genes are significantly upregulated in the presence of azoles in the Δ*afu-182* strain compared to the GMM control. (C) Comparison between CEA10 azole and Δ*afu-182* azole. *rtmA* (orange arrow) and *rtmB* (purple arrow) are significantly upregulated in Δ*afu-182* samples compared to WT in the presence of voriconazole. (D) Comparison between the WT azole and comp-182 azole group. No significant difference in *rtmA* or *rtmB* was observed.

Quantitative reverse transcriptase PCR to assess the mRNA levels of (E) *rtmA* and (F) *rtmB*. Significant upregulation of *rtmA* (3-fold compared to WT, $p<0.0001$, One-Way ANOVA followed by Tukey's post-hoc analysis) and *rtmB* (4.6-fold compared to WT, $p<0.0001$, One-Way ANOVA followed by Tukey's post-hoc analysis) was observed in Δ*afu-182* strains compared to WT in the presence of voriconazole. No significant difference in *rtmA* and *rtmB* expression was observed in the absence of azoles. Groups showing significant differences are marked with p values on the graph (one-way ANOVA, Tukey's post-hoc analysis). Orange arrow – *afub_000050* (*rtmA*) and purple arrow – *afub_000060* (*rtmB*). ns – Not significant

Figure 9. *rtmA* and *rtmB* play a role in fungal azole response. AF strains (A) Δ*rtmA* and comp-*rtmA*, (C) Δ*rtmB* and comp-*rtmB* and (E) Δ*rtmA* Δ*rtmB* were point inoculated in the absence or presence of 0.25 μg/ml of voriconazole. The plates were incubated at 37°C for 48 hours and photographed. The inset shows images taken with a macro lens. After 48 hours, colony diameter was measured and growth ratio of drug over no drug for (B) Δ*rtmA* and comp-*rtmA*, (E) Δ*rtmB* and comp-*rtmB* and (H) Δ*rtmA*Δ*rtmB* (three independent deletion strains) were plotted. One-way ANOVA was used to assess the difference in the mean. Numerical p-values are represented based on Tukey's post-hoc analysis to compare the means of all groups.